POLYMERIZED IONIC LIQUID DERIVED CARBON

A Thesis

by

RUI SUN

Submitted to the Office of Graduate and Professional Studies of
Texas A&M University
in partial fulfillment of the requirements for the degree of

MASTER OF SCIENCE

Chair of Committee,	Yossef A. Elabd
Committee Members,	Jodie L. Lutkenhaus
	Lei Fang
Head of Department,	M. Nazmul Karim

August 2016

Major Subject: Chemical Engineering

ABSTRACT

The development of new carbon-based materials with exquisite control over surface chemistry, carbon structure and form, surface area, pore size, and conductivity is of significant interest for numerous applications, including energy storage (*e.g.*, capacitors). Recently, a few studies have demonstrated the ability to produce carbon from ionic liquids (ILs) and polymerized ionic liquids (PILs), both of which have unique physiochemical properties and result in carbon with various surface chemistries depending on the chemistry of the IL or PIL. However, to date, few studies have explored the relationship between the possible diverse PIL chemistries and the resulting PIL-derived carbon properties. In this study, numerous PILs with various backbone/cation pairings (backbones: ethyl methacrylate, styrene; covalently attached cations: butylimidazolium, trimethylammonium, piperidinium, butylpyrrolidinium, methylpyrrolidinium) were synthesized as carbon precursors. The chemistry and molecular weight of the PILs were characterized using proton nuclear magnetic resonance (^{1}H NMR) spectroscopy, elemental analysis (EA), and gel permeation chromatography (GPC). PIL-derived carbons were produced from this set of PILs *via* pyrolysis at 10 °C/min. The surface chemistry, carbon structure and form, porosity, and conductivity of these PIL-derived carbons were characterized using X-ray photoelectron spectroscopy (XPS), X-ray diffraction (XRD), scanning electron microscopy (SEM), and transmission electron microscopy (TEM). A fundamental investigation into the relationship between PIL chemistry and PIL-derived carbon properties was explored,

along with the subsequent implications on electrode materials for energy storage applications.

ACKNOWLEDGEMENTS

First and foremost, I deeply appreciate my advisor, Dr. Yossef Elabd, for giving me the opportunity to learn from him. It is his guidance and encouragements that help me to improve myself towards a competent researcher. I would also like to express my appreciation to all the previous and present members for the conversations that help me overcome the difficulties, both in research and personal life. Especially thanks to Kelly Meek, for being a role model and mentoring me every step of the way. The conversations with her inspired me and let me keep faith in myself. Thank you to all my thesis committee, Dr. Jodie Lutkenhaus and Dr. Lei Fang, for taking time out of your busy schedule to meet me and review my work. Last but not least, many thanks to all my family and friends that kept encouraging me in the past two years. None of this would be possible without their love and support.

TABLE OF CONTENTS

LIST OF FIGURES

LIST OF TABLES

LIST OF SCHEMES

1. INTRODUCTION AND LITERATURE REVIEW

1.1 Carbon Materials

Carbon materials have attracted extensive interest and investigation for various applications due to its outstanding physical and chemical properties, *i.e.,* accessibility, relatively low cost, numerous forms (powders, fibers, sheets, tubes, monoliths, *etc.*), non-toxicity, controllable porous structure and surface area, high electrical conductivity, chemical stability, *etc.*[1] Carbon materials can be classified into various allotropic forms, such as graphite, diamond-like carbon, amorphous carbon, carbon nanotube, and buckminsterfullerene (C_{60}), *etc*. Different morphologies will result in different physical and chemical properties among the allotropes. For example, carbon with graphite structure, formed by 2D sheets of sp^2 hybridized carbon atoms with hexagonal lattice, exists in soft form and shows outstanding electrical conductivity.[2] Diamond-like carbon contains a significant amount of sp^3 bonds and displays high chemical inertness and hardness.[3] To date, numerious types of carbon with different properties have been investigated, including activated carbon (AC), carbon nanotubes,[4] carbon aerogels, *etc*. AC is typically prepared by two approaches: (1) physical activation (thermal treatment of precursors at high temperature (700-1000 ℃) in oxidizing gas flow (*i.e.,* air, CO_2, steam); (2) chemical activation (treatment of precursors at low temperature (400-700 ℃) with activating agents (H_3PO_4, KOH, NaOH, $ZnCl_2$, *etc.*). The resulting AC with high surface area is a good candidate for energy storage applications, such as supercapacitors. However, Linares-Solano *et al.*[5] reported that mesoporous AC with high surface area

(e.g., >2000 m^2/g) did not obtain high capacitance as expected, which suggested that surface area is not the only factor for improving capacitance. More investigations are necessary in controlling the pore size distribution and surface chemistry of ACs.[1,6,7] Carbon nanotubes (CNTs), classified as single-walled nanotubes (SWNTs) and multiwalled nanotubes (MWNTs), are known for their high electrical conductivity, relatively high surface area, and good mechanical properties. CNTs have showed potential in many applications, including conductive and high-strength composites, energy storage devices, and electron field emission.[4,6] However, retaining the intrinsic properties of individual CNTs on a macroscopic scale is still a challenge for CNT development in the future.[7] Carbon aerogels (CAG), typically generated by pyrolysis of organic aerogels from a sol-gel process, are ultralight porous carbon materials with pore size typically larger than 2 nm. One of the most attractive features of CAGs is that they can be used without binding substances, while the limitation is the relatively high internal resistance caused by the microporosity.

A variety of factors have shown to impact the properties of carbon materials, including pore size and pore size distribution, surface area, and content of heteroatoms. Previous study[1,2,8,9] showed that materials containing both micropores and larger pores are favored as a result of the combination of energy storage realized in micropores and fast mass-transport of electrolytes provided by larger pores. Doping heteroatoms onto carbon materials have also been reported to successfully modify the chemical structure of carbon material and affect conductivity.

1.2 Nitrogen Doped Carbon

Nitrogen-doped carbons with distinct properties have attracted investigations in recent years. Compared to other carbon materials, carbons modified by nitrogen atoms have been observed to possess high conductivity[6,10] and catalytic activity[11,12]. Potential applications of nitrogen-doped carbon are metal-free catalysts for oxygen reduction reaction (ORR)[11] and absorbents for CO_2 capture[13]. Several studies have also proved that electrode materials with heteroatoms (N, O, S, P) introduced into carbon frameworks may further enhance the capacitance,[13-18] conductivity[6,10] and charge-discharge cycleability[17]. For nitrogen-doped carbons, the nitrogen groups in the carbon matrix have an impact on improving the charge mobility of the carbon by changing the electron donor-acceptor characteristics and giving rise to pseudocapacitance by the fast and reversible Faradic redox reactions with ions in electrolytes.[17,19,20]

There are two typical strategies to prepare nitrogen-doped carbons: doping nitrogen onto carbon by post-treatment with nitrogen containing atmosphere, such as ammonia gas/air,[21-25] or carbonization of nitrogen contained precursors.[13,17-20,26] Post-treatment strategies will result in low nitrogen content and inhomogeneous distribution of nitrogen while carbonization strategies provide a more homogeneous product with higher nitrogen content.

Several groups have successfully synthesized nitrogen-doped carbon from the pyrolysis of polymer precursors.[13,18,20,27-29] Hulicova and coworkers[20] reported that melamine was successfully polymerized using fluorine mica template, followed by a pyrolysis at various temperatures in the range of 650-1000 °C. The nitrogen-doped

3

carbon produced at 750 ℃ obtained a maximum gravimetric specific capacitance of 204.8 F g^{-1}. Electrochemical characterization results indicated the presence of pseudocapacitance introduced by the nitrogen sites, where samples generated at higher temperature provides high values of capacitances despite the lower surface areas. The effect of pyridinic nitrogen on the electron donor-acceptor properties was also suggested in this study.

Wei *et al.*[13] synthesized nitrogen-doped mesoporous carbon by solvent evaporation induced self-assembly process using soluble resol as a carbon source, dicyandiamide as the nitrogen source and commercial PEO-b-PPO-b-PEO triblock copolymer as the template. Pyrolysis took place at 600 ℃ resulting in ordered mesoporous carbons with tunable pore size (3.1 to 17.6 nm), high surface area (494 to 586 m^2 g^{-1}), high nitrogen content (up to 13.1 wt%), which show high CO_2 capture and high specific capacitance for supercapacitor application.

Li *et al.*[18] generated partially graphitized carbons from eggwhite-derived proteins with pore sizes of 20 to 30 nm, high surface area (805.7 m^{2}g^{-1}), and high nitrogen content (10.1 wt%). Electrochemical measurements showed a reversible lithium storage capacity of 1780 mA h g^{-1}, as well as a capacitance of 390 F g^{-1} and an excellent charge-discharge cycle life of 7% loss after 10000 cycles in a supercapacitor.

Numerous carbon precursors have been employed in the study of synthesizing nitrogen-doped carbon material. Poly(acrylonitrile) is one of the most popular candidates as a carbon precursor due to its high amount of carbon residue. There are many reports on poly(acrylonitrile) (PAN) as a precursor for nitrogen-doped carbon.[27-29] Yuping Wu

4

and coworkers[27] synthesized PAN by free radical polymerization and carbonized the polymer precursor at 1000 ℃ to prepare carbon powders as a carbon anode for a lithium secondary battery. Park *et al.*[28] successfully prepared electrospun PAN nanofibers and carbonized the nanofibers at 1000 ℃ to achieve carbon nanofibers for application to polymer electrolyte membrane fuel cells (PEMFCs).

Zhong *et al.*[29] synthesized poly(n-butyl acrylate) (PBA)-b-PAN block copolymer by atom transfer radical polymerization. A thermal stabilization step took place at 280 ℃ under air flow followed by carbonization at 700 ℃, where PBA block burnt out leaving a porous structure behind. Figure 1.1 shows the preparation of copolymer-templated nitrogen-enriched porous carbons (CTNC). CTNC with high surface area and high capacitance per surface area was obtained as promising material for capacitor application.
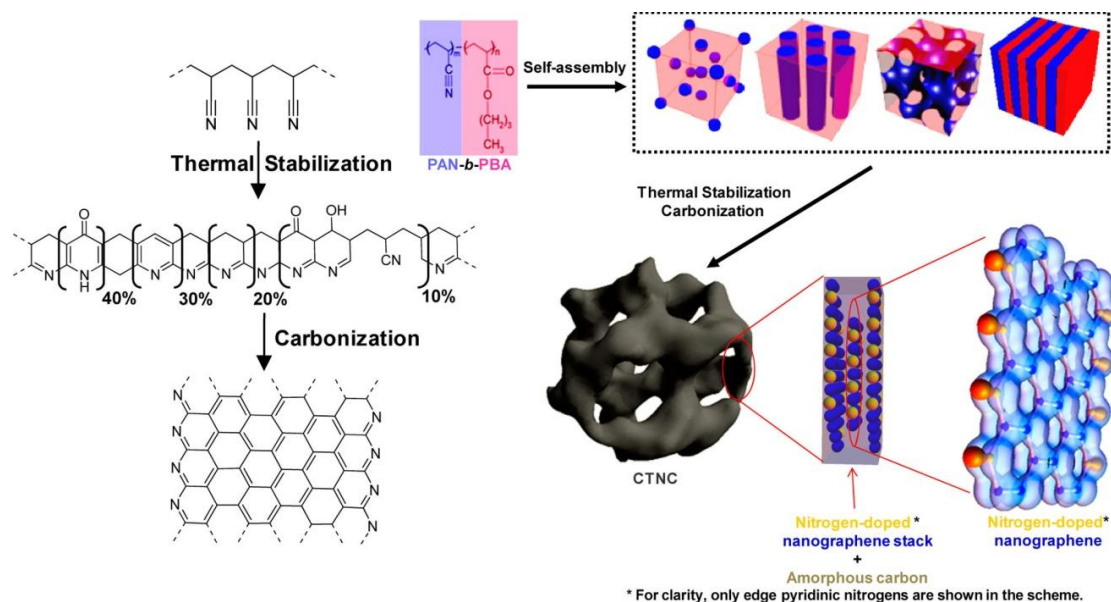
Figure 1.1 Preparation of CTNC. Figure adapted from reference [29]

1.3 Ionic Liquids (ILs) as Nitrogen-doped Carbon Precursors

Recently, ionic liquids (ILs) have been investigated as nitrogen-doped carbon precursors. ILs are defined as salts that contain an organic cation and an organic or inorganic anion and typically have melting point lower than 100 ℃. They are also known as room temperature ionic liquids (RTILs) when the melting point is below room temperature. ILs have been extensively investigated due to their remarkable physiochemical properties, including negligible volatility, nonflammability, high ionic conductivity, outstanding chemical and thermal stability, and a wide electrochemical window, *etc*. Ethylammonium nitrate, the first IL, was introduced in 1914 by Paul Walden.[30] Since then, an increasing number of applications of ILs have been developed and investigated in various fields, including catalysis,[31] polymer chemistry,[32] electrochemistry,[33,34] analytical chemistry,[35] *etc*. Figure 1.2 shows chemical structures of some representative cations and anions used in ILs.
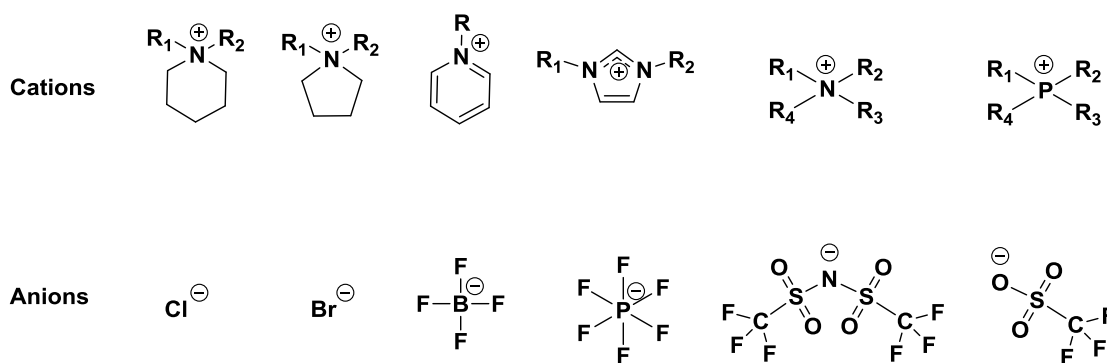
Figure 1.2 Representative chemical structures of cations and anions in ILs.

Only few recent studies have explored ILs as precursors for nitrogen-doped carbon.[11,36-39] Benefiting from the negligible volatility of ILs, a higher yield of nitrogen-doped carbon can be achieved using ILs as precursors. Antonietti and coworkers[36] found that ILs can be precursors for synthesizing mesoporous nitrogen-doped carbon in a mesoporous silica template at 1000 ℃. With the advantage of negligible volatility, a high mass yield was achieved with almost no loss in IL precursor before the occurrence of decomposition processes. A new type of N-doped graphitic carbon with high conductivity was achieved and showed potentials as nanoelectronic materials. Antonietti and coworkers[11] also prepared mesoporous N-doped carbon materials with high surface areas up to 1500 m^2 g^{-1} by the carbonization of nucleobases dissolved in an IL (1-ethyl-3-methylimidazolium dicyanamide) and suggested its potential application as catalyst for ORR.

Fechler and coworkers[39] reported a facile approach to synthesize composites of titanium, vanadium, and titanium−vanadium nitride nanoparticles embedded nitrogen-doped carbon. IL, 1-butyl-3-methyl-pyridinium dicyanamide (BMP-DCA), was used as N-doped carbon precursor for thermal treatment. $TiCl_4$ or $VOCl_3$ was dissolved in ionic liquid as the metal source.

1.4 Polymerized Ionic Liquids (PILs) as Nitrogen-doped Carbon Precursors

Polymerized ionic liquids (PILs) are a distinct type of polymer that typically contains a covalently attached IL cation exchanged with its anion. Ohno[40] first synthesized a polymerized ionic liquid (PIL) by direct polymerization of the IL monomer, 1-ethyl-3-

vinylimidazolium bis(trifluoromethanesulfonylimide) (EtVyIm$^+$TFSI$^-$). Different from ILs, where both cations and anions are mobile, the cations of PILs are constrained to each repeating unit of the polymer chain. Unlike other ion-containing polymers that are typically restricted to high glass transition temperatures due to strong electrostatic ion pair interactions, PILs can possess low glass transition temperatures due to weak electrostatic ion pair interactions, while maintaining high charge densities.[41] Thus, numerous applications of PILs have been investigated, including polymer electrolytes, solid ionic conductors, sorbents, dispersing agents, precursors for carbon materials, *etc*.

1.4.1 PIL Synthesis

The synthesis of PILs can be performed *via* two typical approaches: direct polymerization of an IL monomer or chemical modification on a non-ionic polymer precursor. Polymerization of IL monomers (ILs that contain polymerizable segments) introduces a straightforward approach to synthesis PILs, however, the limitation of this strategy is that the resulting charged polymers have a great possibility to aggregate in solution and lead to difficulty in measuring molecular weight by conventional methods, such as gel permeation chromatography (GPC). Meanwhile, the strategy of chemical modification provides a facile approach to determine the molecular weight of PILs by calculation from the molecular weight of non-ionic precursor measured by GPC. Generated by functionalization, the PILs will retain the chemical structure, degree of polymerization (DP), and polydispersity index (PDI) from the non-ionic polymer precursor and achieve structures, which are inaccessible by direct polymerization.

To date, various polymerization techniques have been applied to both PIL synthesis strategies, including conventional free radical polymerization, controlled/living radical polymerization, ring opening metathesis polymerization, *etc*. For each method, various kinds of cations and couterions can be applied to synthesize numerous PILs with different properties. Table 1.1 shows some examples of PILs synthesized by different polymerization techniques.

Table 1.1 Examples of PILs and their polymerization techniques.
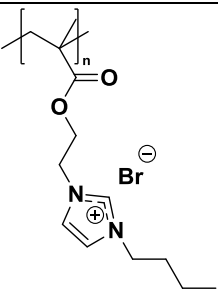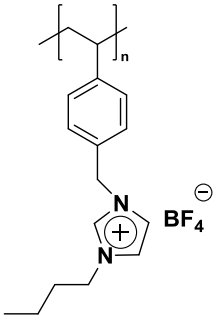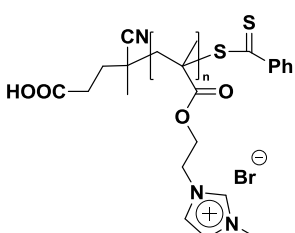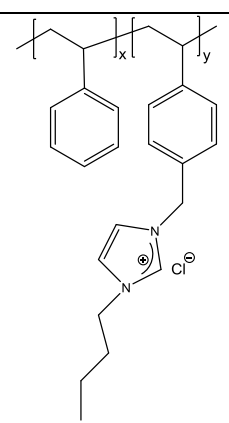
Polymerization Techniques		Example Structures	References	Additional References
Conventional free radical polymerization			42	40,43-47
Controlled/living radical polymerization	Atom transfer radical polymerization (ATRP)		48	49-53

Table 1.1 Continued.

Polymerization Techniques		Example Structures	References	Additional References
Controlled/living radical polymerization	Reversible addition-fragmentation chain transfer (RAFT)		54	41,48,55-60
	Nitroxide-mediated polymerization (NMP)		61	62-65

Conventional free radical polymerization technique is one of the most popular techniques in PIL synthesis. Ohno[40] first synthesized a PIL from the IL monomer, EtVyIm$^+$TFSI$^-$, in 1998. Ohno and coworkers[43] also prepared N-vinylimidazolium tetrafluoroborate (VyImBF$_4$) and polymerized to obtain poly(VyImBF$_4$). Ye and Elabd[42] successfully prepared imidazolium-based PILs with different anion types (bis(trifluoromethanesulfonyl) imide (TFSI$^-$), tetrafluoroborate (BF$_4^-$),

trifluoromethanesulfonate (T_f^-), and hexafluorophosphate (PF_6^-)) and investigated the impact of anion type on the chemical, thermal, and conductive properties. Shaplov *et al*[44] produced a series of bis(trifluoromethylsulfonyl)amid-based ionic monomers with various cations (imidazolium, ammonium and pyrrolidinium cation) followed by free radical polymerization.

Controlled/living radical polymerization is chain growth polymerization that proceeds in the absence of irreversible chain transfer and termination steps.[66] With the advantage of controlled radical polymerization, polymers with controlled molecular weight distribution and chemical structure can be designed. Several controlled radical polymerization methods have been developed, such as atom transfer radical polymerization (ATRP), reversible addition-fragmentation chain transfer (RAFT) polymerization, nitroxide-mediated free radical polymerization (NMP), *etc*.

ATRP was first employed to produce PIL homopolymers by Shen and coworkers[49] using 2-(1-butylimidazolium-3-yl)ethylmethacrylate tetrafluoroborate (BIMT) as the ionic monomer and CuCl catalyst proved to be an efficient catalyst for highly controlled polymerization. Shen and coworkers[48] also synthesized PILs *via* ATRP using 1-(4-vinylbenzyl)-3-butyl imidazolium tetrafluoroborate (VBIT) and 1-(4-vinylbenzyl)-3-butyl imidazolium hexafluorophosphate (VBIH) as ionic monomers, respectively. Pei and coworkers[52] successfully prepared well-defined poly[1-(4-vinylbenzyl)-3-butylimidazolium hexafluorophosphate] ($PVBIm-PF_6$) brushes with tunable wettability *via* surface initiated ATRP. Recently, Matyjaszewski and coworkers[50] reported well-defined PILs synthesized by activators regenerated by electron transfer (ARGET) ATRP

using 1-(4-vinylbenzyl)-3-butylimidazolium bis(trifluoromethylsulfonyl)imide ($VBBI^+Tf_2N^-$) as the ionic monomer.[53]

Extensively investigations on synthesizing PIL homopolymers and block copolymers *via* RAFT polymerization have been demonstrated.[48,54-60] Gnanou *et al.*[54] successfully polymerized three different ionic monomers, respectively, to prepare PIL homopolymers and subsequently copolymerized the resulting PILs with methacrylic acid or acrylamide to obtain PIL block copolymers. All the polymerizations were performed *via* RAFT polymerization technique. Shen and coworkers[48] reported the synthesis of PVBIT by polymerizing p-chloromethylstyrene *via* RAFT polymerization followed by quaternization with N-butylimidazole and an anion-exchange reaction to exchange to BF_4^- form. Elabd, Winey, and coworkers[58] recently synthesized a PIL block copolymer, poly(MMA-b-MEBIm-Br), *via* RAFT polymerization. One block was polymerized from a nonionic monomer methylmethacrylate (MMA), while the other block was polymerized from an IL monomer, (1-[(2-methacryloyloxy)ethyl]-3-butylimidazolium bromide) (MEBIm-Br).

Several groups have also synthesized PIL homopolymers and block copolymers *via* NMP technique. Pei *et al.*[65] synthesized poly(allyltriphenylphosphonium hexafluorophosphate) ($PATPP-PF_6$) brushes *via* surface-initiated NMP technique. PIL block copolymer precursor, polystyrene-block-polychloromethylstyrene (PS-b-PCMS), was prepared by Balsara and coworkers[61] *via* NMP followed by quaternization of PCMS block with trimethylammonium chloride and n-butylimidazolium chloride, respectively.

1.4.2 PIL Carbonization

There are several recent reports on PILs as carbon precursors.[37,57,67-69] Studies showed that higher carbon yields can be obtained compared to IL-derived nitrogen-doped carbon due to the additional backbone immobilization without the use of additional nitrile groups. Antonietti and coworkers[37] successfully demonstrated that a template-free synthesis of carbon nanostructures with high electric conductivity can be achieved using IL monomers and PILs as carbon precursors. Four different kinds of imidazolium-based IL monomers were involved in this study and two kinds of PILs were synthesized through free radical polymerization. The presence of $FeCl_2$ was proved to have influence on controlling both the chemical structure and the texture morphology of the graphitization process. 900 ℃ is a threshold temperature that enables the development of large surface area and low resistance. A comparably well-developed mesoporous carbon structure was achieved by the removal of the remainder of $FeCl_2$ byproduct *via* an acid etching process.

Antonietti and coworkers[67] reported that by carbonizing electrospun PILs, highly conductive nitrogen-doped carbon fibers were achieved. Two kinds of PILs, poly(3-allyl-1-vinylimidazolium dicyanamide) (PAVIm-DCA) and poly(1-allyl-4-vinylpyridinium dicyanamide) (PAVP-DCA) were prepared from chemical modifications of poly(1-vinylimidazole) (PVIm) made from free radical polymerization and poly(4-vinyl-pyridine) (P4VP) polymers, respectively. 6.33% and 8.00% of nitrogen were doped on PAVIm-DCA and PAVP-DCA, respectively, and achieved a conductivity of 200 ± 60 S cm^{-1}. Antonietti and coworkers[57] also successfully synthesized double

hydrophilic block copolymers containing poly(N-isopropylacrylamide) (PNIPAAm) or poly(N,N-dimethylacryamide) (PDMA) as a non-ionic segment and PIL as a hydrophilic segment *via* the RAFT/MADIX (reversible addition-fragmentation chain-transfer/macromolecular design *via* the interchange of xanthates) process. Four 1-vinylimidazolium-based IL monomers with different alkyl substitutes and anions were included in this block copolymer synthesis. $PNIPAAm_{60}$-b-PIL/d_{11} were successfully employed as a carbon precursor with the presence of metal salts, such as $FeCl_2 \cdot 4H_2O$ and $CrCl_3 \cdot 6H_2O$.

Yuan and coworkers[68] successfully synthesized mesoporous PIL copolymer monoliths with high specific surface area (935 m^2/g^{-1}) and high pore volumes by solvothermal copolymerization of divinylbenzene and two monomeric ILs, 1-ethyl-3-vinylimidazolium bromide (EVIBr) and 1-butyl-3-vinylimidazolium hexafluorophosphate ($BVIPF_6$), respectively. The application for microporous carbon precursor and polymer-supported catalyst were also suggested. Yuan and coworkers[69] also reported the synthesis of poly[3-cyanomethyl-1-vinylimidazolium bis(triuoromethanesulfonyl)imide] ($PCMVImTf_2N$) using 3-cyanomethyl-1-vinylimidazolium bromide (CMVImBr) as a monomer *via* conventional free radical polymerization followed by anion exchange methathesis. Carbonization was performed at intermediate temperatures (500 to 800 ℃) and resulted in micro/mesoporous nitrogen-doped carbons product without using a template or activation agent.

1.5 Summary and Outline

The studies above demonstrate the ability to produce carbon from ILs and PILs, however, to date, few studies have explored the relationship between the possible diverse PIL chemistries and the resulting PIL-derived carbon properties. As potential influence on the morphology of the resulting carbon may exist with different chemical structure of both polymer backbone and cation, it is of significant importance to compare the morphology and properties of PIL-derived carbons between various cations with the same polymer backbone, as well as compare the influence of various polymer backbones with same cation. In this study, numerous PILs with various backbone/cation pairings (backbones: ethyl methacrylate, styrene; covalently attached cations: butylimidazolium, trimethylammonium, piperidinium, butylpyrrolidinium, methylpyrrolidinium, pyrrolidinium) were synthesized as carbon precursors. Section 2 focuses on the synthesis and characterization of these PILs. The relationship between the backbone/cation type and thermal properties is discussed in this section. Section 3 focuses on the nitrogen-doped carbons derived from this set of PILs synthesized in Section 2. PIL-derived carbons were produced *via* pyrolysis at a heating rate of 10 ℃/min. The carbon structure, form, porosity, surface chemistry and conductivity of the PIL-derived carbons were characterized. This study provides a fundamental investigation into the relationship between PIL chemistry and PIL-derived carbon properties.

15

2. SYNTHESIS AND CHARACTERIZATION OF POLYMERIZED IONIC LIQUIDS WITH VARIOUS BACKBONES AND CATIONS

2.1 Introduction

Recently, several studies have demonstrated the ability to produce carbons with rich nitrogen surface chemistry from ILs[12,36,37,39] and PILs[37,57,67-69]. Nitrogen-doped carbon derived from ILs and PILs with high surface areas and high conductivity have potential for numerous applications. However, to date, few studies have explored the relationship between the possible diverse PIL chemistries and the resulting PIL-derived carbon properties, where there is a diverse set of cation and anion PIL chemistries available. As potential influence on the morphology of the resulting carbon may exist with different chemical structure of both polymer backbone and cation, it is of great significance to compare various cations on the same polymer backbone, as well as compare different polymer backbones on same cation. As a result, it is necessary to further explore the influence of backbone and cation type and determine the promising chemistry for PIL-derived carbons as potential materials for future energy storage devices and other applications.

In this section, numerous PILs with various backbone/cation pairings (backbones: ethyl methacrylate, styrene; covalently attached cations: butylimidazolium, trimethylammonium, piperidinium, butylpyrrolidinium, methylpyrrolidinium) were synthesized as carbon precursors (see Scheme 2.1). The chemistry and molecular weight of the PILs were characterized *via* ^{1}H NMR spectroscopy, elemental analysis (EA), and

gel permeation chromatography (GPC). The glass transition temperatures of the PILs were determined by differential scanning calorimeter (DSC) and the polymer degradation temperatures were characterized by thermal gravimetric analysis (TGA). The results establish a further understanding on the relationship between various chemistries of PILs and their thermal properties and provide insight on the subsequent carbonization experiments for the next section.

Scheme 2.1 Chemical structures of PILs with various backbone/cation pairings.

Poly(MEPip-TFSI)   Poly(MEBP-TFSI)

Poly(VBBIm-TFSI)   Poly(VBTMA-TFSI)   Poly(VBPip-TFSI)

Poly(VBBP-TFSI)   Poly(VBMP-TFSI)
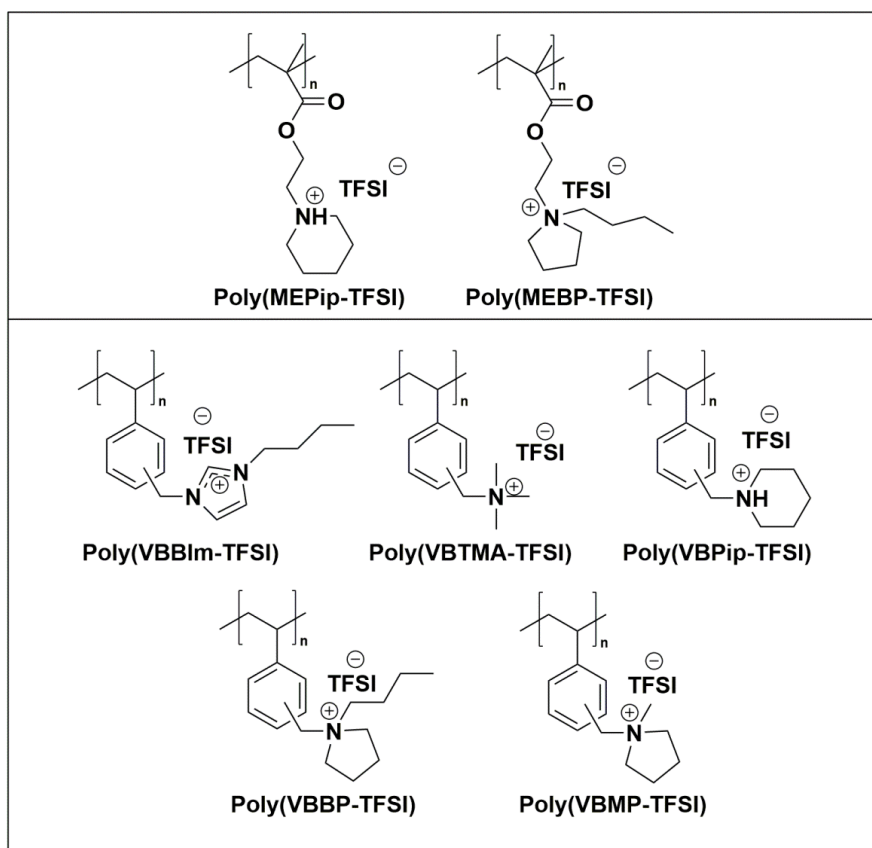
2.2 Experimental Method

2.2.1 Materials

Methacrylol chloride (97%, contains ~200 ppm monomethyl ether hydroquinone as stabilizer), 2-bromoethanol (95%), triethylamine (≥99%), dichloromethane (anhydrous, ≥99.8%, contains 40-150 ppm amylene as stabilizer), magnesium sulfate (anhydrous, ReagentPlus®, ≥99.5%), sodium bicarbonate (powder, BioReagent, for molecular biology, suitable for cell culture, suitable for insect cell culture), 4-cyano-4-(phenylcarbonothioylthio)pentanoic acid (chain transfer agent (CTA), >97%, HPLC), tetrahydrofuran (THF, ≥99.9%), methanol (≥99.9%, HPLC), poly(vinylbenzyl chloride) (60/40 mixture of 3- and 4-isomers, M_n ~55.0 kg mol^{-1}, M_w ~100 kg mol^{-1} by GPC/MALLS), N, N-dimethylformamide (DMF, ACS Reagent, ≥99.8%), 1-butylimidazole (98%), trimethylamine solution (45 wt% in H_2O), 1-butylpyrrolidine (98%), piperidine (≥99.5%, purified by redistillation), 1-methylpyrrolidine (97%), pyrrolidine (99%), hexane (anhydrous, 95%), diethyl ether (anhydrous, ≥99.7%, contains 1 ppm BHT inhibitor), acetone (ACS reagent, ≥99.5%), dimethyl sulfoxide-d_6 (DMSO-d_6, 99.9 atom % D, contains 0.03% v/v TMS), acetonitrile-d_3 (CD$_3$CN, 99.9 atom % D) and deuterium oxide (D_2O, 99.98 atom% D) was purchased from Sigma-Aldrich and used as received without further purification. Bis(trifluoromethane)sulfonimide lithium salt (LiTFSI) (98+%) was purchased from Alfa Aesar and used as received without further purification. Azobis(isobutyronitrile) (AIBN, 98%, Sigma-Aldrich) was purified by recrystallization twice from methanol. Ultrapure deionized (DI) water with resistivity *ca.* 16 MΩ cm was used as appropriate.

2.2.2 Synthesis of 2-Bromoethyl Methacrylate Monomer (BrEMA)

The synthesis of the monomer 2-bromoethyl methacrylate (BrEMA) was performed according to literature.[42] A representative synthesis is given as follows: 39.37 g (0.315 mol) 2-bromoethanol and 75 mL of dicholoromethane (DCM) were added into a 500 mL three-neck flask. The reactor was placed in an ice bath and well-sealed with septum under nitrogen flow under continuous mixing. A mixture of 33.64 g (0.33 mol) triethylamine and 75 mL DCM was slowly added into the reaction flask through an addition funnel, followed by adding a mixture of 31.36 g (0.30 mol) methacryloyl chloride and 50 mL DCM dropwise using an addition funnel. The reactor was then removed from ice bath and continuously stirred at room temperature for 20 h. Followed by a filtration and removal of the solid phase, the liquid phase was washed with 250 mL of saturated sodium bicarbonate ($NaHCO_3$) three times and followed by three times washing with 250 mL DI water using a separating funnel. The organic phase was retained and dried with magnesium sulfate to remove residual water. Magnesium sulfate was then filtered followed by removing DCM from the organic mixture by vacuum and the resulting light-yellow monomer was stored in refrigerator for later use. Yield: 36.35 g (0.188 mol) (59.7%). ^{1}H NMR (Mercury 300 MHz, $CDCl_3$, 23 °C) δ (ppm): 6.17 (s 1H, HCH=C(CH_3)), 5.63(s, 1H, HCH=C(CH_3)), 4.46 (t, 2H , O-CH_2-CH$_2$-Br), 3.56 (t, 2H,O-CH$_2$-CH_2-Br), 1.97 (s, 3H, CH$_2$=C(CH_3)).

Scheme 2.2 Synthesis of PILs: (a) poly(MEX-TFSI)[a], (b) poly(VBX-TFSI)[b], X^+ = various cations (A-E).

(a)

(b)

$X^{\oplus}$ = (A) Pip (B) BP (C) TMA (D) BIm (E) MP

(1a) CTA, AIBN, 70°C, 5h; (2A) Piperidine, DMF, 80°C, 48h; (2B) 1-butyl pyrrolidine, DMF, 80°C, 48h; (2C) Trimethylamine (aqueous), DMF, rt, 48h; (2D) 1-butyl imidazole, DMF, 80°C, 48h; (2E) 1-methyl pyrrolidine, DMF, 65°C, 96h (3)LiTFSI, H₂O, rt, 48 h
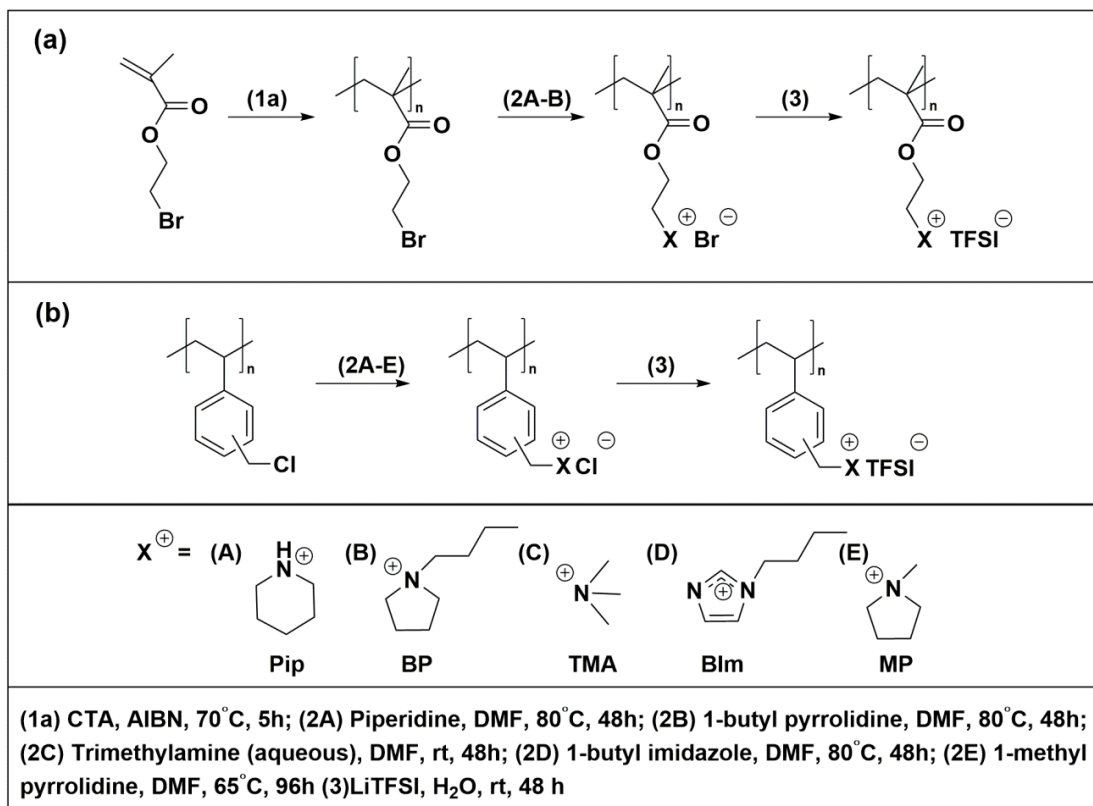
2.2.3 Synthesis of Poly(BrEMA)

RAFT polymerization was utilized to synthesize the non-ionic homopolymer precursor poly(BrEMA). The procedure is shown in Scheme 2.2 (1a). An example reaction: 15.0120 g of BrEMA (77.7 mmol), 72.7 mg of CTA (0.260 mmol), 4.4 mg of AIBN (0.0268 mmol), and 2.9985 g tetrahydrofuran (THF) were combined in a 250 mL single-neck Schlenk flask under continuous mixing. The reactor neck was well-sealed with septum and subjected to three freeze-pump-thaw degassing cycles. Followed by sealing the reactor arm and thawing in water bath, the reaction was carried out under N_2 at 70 °C

for 5 h. The resulting polymer was precipitated in methanol, filtered and then dried under vacuum in an oven at room temperature for 24 h. Yield: 6.04 g of pink solid particles (40%). ^{1}H NMR (Mercury 300 MHz, CDCl$_3$, 23 °C) δ (ppm): 4.47-4.19 (s, 2H, O-CH_2-CH$_2$-Br), 3.66-3.47 (s, 2H,O-CH$_2$-CH_2-Br), 2.12-1.84 (d, 3H, CH$_2$-C(CH_3)), 1.12 (s, 1H, HCH-C(CH$_3$)), 0.98 (s,1H, HCH-C(CH$_3$)) (NMR, Figure 2.1). GPC (THF, 40 °C): M_n = 19.02 kg mol^{-1}, M_w/M_n = 1.82 (against PS standards).

2.2.4 Synthesis of Poly(MEPip-TFSI)

The synthesis procedure of the PIL, poly(MEPip-TFSI) [MEPip-TFSI = 1-[(2-methacryloyloxy) ethyl]-piperidinium bis(trifluoromethane) sulfonimide], is shown in Scheme 2.2 (2a(A)). An example reaction: 1.0018 g (5.19 mmol) of poly(BrEMA) was dissolved in 18 mL DMF in a 125 mL flask. 0.8822 g (10.36 mmol) of piperidine (poly(BrEMA)/piperidine, 1/2 mol/mol) was slowly added dropwise into the flask. The reaction was performed at 80 °C for 48 h. The resulting polymer was precipitated in hexane followed by extensive washing in hexane multiple times. The solid polymer was dried under vacuum in an oven at room temperature for 24 h resulting in a yield of 1.7722 g (6.37 mmol) orange solid particles (122.7%). Subsequently, anion exchange metathesis was performed on the dried polymer, poly(MEPip-Br), to exchange from Br$^-$ to TFSI$^-$ form. 11.1453 g (38.8 mmol) of LiTFSI was stirred in 100 mL of DI water and added dropwise into 1.2005 g (4.32 mmol) of poly(MEPip-Br) dispersed aqueous solution (poly(MEPip-Br)/LiTFSI, 1/9 mol/mol). The solid state anion exchange reaction was carried out at room temperature for 48 h followed by washing with DI water for 72

h. The anion exchanged polymer, poly(MEPip-TFSI), was filtered and dried under vacuum in an oven at room temperature for 24 h. The efficacy of anion exchange from Br⁻ to TFSI⁻ was confirmed by EA and determined to be ~100% efficient. Yield: 0.9073 g of solid particles (70.6%). ^{1}H NMR (500 MHz, acetonitrile-d$_3$, 23 °C) δ (ppm): 4.47-3.92 (s, 2H, N-CH$_2$-CH_2-O), 3.36-2.23 (m, 11H, (CH$_2$)$_2$-NH-CH$_2$-CH$_2$-O, N-CH_2-CH_2-CH$_2$-CH_2-CH$_2$-N, N-CH_2-CH$_2$-O), 1.79-1.38 (m, 5H, N-CH$_2$-CH$_2$-CH_2-CH$_2$-CH$_2$-N, CH_2-C(CH_3)), 1.16-0.73 (s, 2H, CH_2-C(CH$_3$)). (NMR, Figure 2.1). EA calculated: C, 32.64; H, 4.21; N, 5.86; Br, 0.00; S, 13.40; F, 23.83. Found: C, 43.62; H, 5.86; N, 5.74; Br, 0.00; S, 8.97; F, 14.62.

2.2.5 Synthesis of Poly(MEBP-TFSI)

The synthesis procedure of the PIL, poly(MEBP-TFSI) [MEBP-TFSI = 1-[(2-methacryloyloxy) ethyl]-1-butylpyrrolidinium bis(trifluoromethane) sulfonimide], is shown in Scheme 2.2 (2a(B)). An example reaction: 1.0004 g (5.18 mmol) of poly(BrEMA) was dissolved in 12 mL DMF in a 125 mL flask. 1.39 g (10.93 mmol) of 1-butylpyrrolidine (poly(BrEMA)/1-butylpyrrolidine, 1/2 mol/mol) was slowly added dropwise into the flask. The reaction was performed at 80 °C for 48 h. The resulting polymer was precipitated in hexane followed by extensive washing in hexane multiple times. The solid polymer was dried under vacuum in an oven at room temperature for 24 h resulting in a yield of 1.5389 g (4.81 mmol) brown solid particles (92.8%). Subsequently, anion exchange metathesis was performed on the dried polymer, poly(MEBP-Br), to exchange from Br⁻ to TFSI⁻ form. 8.0905 g (28.2 mmol) of LiTFSI

was stirred in 50 mL of DI water and added dropwise into 1.0026 g (3.13 mmol) of poly(MEBP-Br) aqueous solution (poly(MEBP-Br)/LiTFSI, 1/9 mol/mol). The reaction was carried out at room temperature for 48 h followed by washing with DI water for 72 h. The anion exchanged polymer, poly(MEBP-TFSI), was filtered and dried under vacuum in an oven at room temperature for 24 h. The efficacy of anion exchange from Br⁻ to TFSI⁻ was confirmed by EA and determined to be ~100% efficient. Yield: 1.1510 g of solid particles (70.6%). ^{1}H NMR (500 MHz, Acetonitrile-d_3, 23 °C) δ (ppm): 4.59-4.07 (s, 2H, N-CH$_2$-CH_2-O), 3.88-3.42 (s, 6H, N-CH_2-CH$_2$-CH$_2$-CH_2-N, N-CH_2-CH$_2$-CH$_2$-CH$_3$), 3.42-3.11 (s, 2H, N-CH_2-CH$_2$-O), 2.38-2.09 (s, 4H, N-CH$_2$-CH_2-CH_2-CH$_2$-N), 1.78-1.62 (s, 2H, N-CH$_2$-CH_2-CH$_2$-CH$_3$), 1.46-1.30 (s, 3H, CH$_2$-C(CH_3)), 1.16-0.80 (m, 7H, N-CH$_2$-CH$_2$-CH_2-CH_3, CH_2-C(CH$_3$). (NMR, Figure 2.1). EA calculated: C, 36.92; H, 5.03; N, 5.38; Br, 0.00; S, 12.32; F, 21.90. Found: C, 38.16; H, 5.13; N, 5.04; Br, 0.00; S, 12.32; F, 20.14.

2.2.6 Synthesis of Poly(VBPip-TFSI)

The non-ionic polymer, PVBC, was used as precursor for the synthesis of styrene backbone PILs. The general procedure included functionalization of PVBC to form an ionic homopolymer followed by an anion exchange metathesis. The synthesis procedure of poly(VBPip-TFSI) [VBPip= vinylbenzylpiperidinium] is shown in Scheme 2.2 (2b(A)). An example reaction: 2.0062 g (13.15 mmol) of PVBC was dissolved in 25 mL DMF in a 125 mL flask. 2.27 g (26.66mol) of piperidine (PVBC/piperidine, 1/2 mol/mol) was slowly added dropwise into the flask. The reaction was carried out at 80 °C for 48 h.

The resulting polymer was precipitated in hexane and subsequently washed in hexane multiple times. The solid polymer was dried under vacuum in an oven at room temperature for 24 h yielding 4.0248 g (16.93 mmol) light yellow solid particles (128.7%). Subsequently, anion exchange metathesis was performed on the dried polymer, poly(VBPip-Cl), to exchange from Cl⁻ to TFSI⁻ form. 16.1930 g (56.4 mmol) of LiTFSI was stirred in 100 mL of DI water and added dropwise into 1.5032 g (6.32 mmol) of poly(VBPip-Cl) dispersed aqueous solution (poly(VBPip-Cl)/LiTFSI, 1/9 mol/mol). The reaction was carried out at room temperature for 48 h followed by washing with DI water for 72 h. The anion exchanged polymer, poly(VBPip-TFSI), was filtered and dried under vacuum in an oven at room temperature for 24 h. The efficacy of anion exchange from Cl⁻ to TFSI⁻ was confirmed by EA and determined to be ~100% efficient. Yield: 1.5414 g (3.19 mmol) of solid polymer (50.5%). ^{1}H NMR (500 MHz, DMSO-d$_6$, 23 ℃) (NMR, Figure 2.1). EA calculated: C, 39.83; H, 4.18; N, 5.81; Cl, 0.00; S, 13.29; F, 23.63. Found: C, 50.54; H, 5.16; N, 5.75; Cl, 0.00; S, 9.58; F, 17.16.

2.2.7 Synthesis of Poly(VBBP-TFSI)

The non-ionic polymer, PVBC, was used as a precursor for the synthesis of styrene backbone PILs. The general procedure included functionalization of PVBC to form an ionic homopolymer followed by an anion exchange metathesis. The synthesis procedure of poly(VBBP-TFSI) [VBBP= vinylbenzylbutylpyrrolidinium] is shown in Scheme 2.2 (2b(B)). An example reaction: 2.0006 g (13.11 mmol) of PVBC was dissolved in 25 mL DMF in a 125 mL flask. 3.34 g (26.25 mol) of 1-butyl pyrrolidine (PVBC/1-butyl

pyrrolidine, 1/2 mol/mol) was slowly added dropwise into the flask. The reaction was carried out at 80 ° C for 48 h. The resulting polymer was precipitated in hexane and subsequently washed in hexane multiple times. The solid polymer was dried under vacuum in an oven at room temperature for 24 h yielding 4.21 g (15.04 mmol) brown solid particles (114.7%). Subsequently, anion exchange metathesis was performed on the dried polymer, poly(VBBP-Cl), to exchange from Cl$^-$ to TFSI$^-$ form. 13.8799 g (48.3 mmol) of LiTFSI was stirred in 100 mL of DI water and added dropwise into 1.5033 g (5.37 mmol) of poly(VBBP-Cl) aqueous solution (poly(VBBP-Cl)/LiTFSI, 1/9 mol/mol). The reaction was carried out at room temperature for 48 h followed by washing with DI water for 72 h. The anion exchanged polymer, poly(VBBP-TFSI), was filtered and dried under vacuum in an oven at room temperature for 24 h. The efficacy of anion exchange from Cl$^-$ to TFSI$^-$ was confirmed by EA and determined to be ~100% efficient. Yield: 2.2247 g (4.24 mmol) of solid polymer (79.0%). ^{1}H NMR (500 MHz, Acetonitrile-d$_3$, 23 °C) δ (ppm): 7.39-6.12 (m, 4H, C$_6$H$_4$), 4.46-3.74 (m, 2H, C$_6$H$_4$-CH$_2$-N), 3.56-3.06 (s, 4H, N-CH$_2$-CH$_2$-CH$_2$-CH$_2$-N), 3.06-2.62 (s, 2H, N-CH$_2$-CH$_2$-CH$_2$-CH$_3$), 2.23-1.06 (m, 11H, N-CH$_2$-CH$_2$-CH$_2$-CH$_2$-N, CH$_2$-CH, N-CH$_2$-CH$_2$-CH$_2$-CH$_3$, CH$_2$-CH, N-CH$_2$-CH$_2$-CH$_2$-CH$_3$), 1.01-0.72 (s, 3H, N-CH$_2$-CH$_2$-CH$_2$-CH$_3$) (NMR, Figure 2.1). EA calculated: C, 43.51; H, 5.00; N, 5.34; Cl, 0.00; S, 12.23; F, 21.73. Found: C, 43.78; H, 5.04; N, 5.49; Cl, 0.00; S, 12.05; F, 21.46.

2.2.8 Synthesis of Poly(VBTMA-TFSI)

The non-ionic polymer, PVBC, was used as a precursor for the synthesis of styrene backbone PILs. The general procedure included functionalization of PVBC to form an ionic homopolymer followed by an anion exchange metathesis. The synthesis procedure of poly(VBTMA-TFSI) [VBTMA= vinylbenzyltrimethylammonium] is shown in Scheme 2.2 (2b(C)). An example reaction: 3.0109 g (19.73 mmol) of PVBC was dissolved in 15 mL DMF in a 125 mL flask. 12.91 g (98.28 mol) of 45 wt% trymethylamine aqueous solution (PVBC/trymethylamine, 1/5 mol/mol) was slowly added dropwise into the flask. The reaction was carried out at room temperature for 48 h. The resulting polymer was precipitated in diethyl ether and subsequently washed in diethyl ether multiple times. The solid polymer was dried under vacuum in an oven at room temperature for 24 h yielding 4.8121 g (22.73 mmol) white solid particles (115.2%). Subsequently, anion exchange metathesis was performed on the dried polymer, poly(VBTMA-Cl), to exchange from Cl$^-$ to TFSI$^-$ form. 24.3439g (84.80 mmol) of LiTFSI was stirred in 100 mL of DI water and added dropwise into 2.0040 g (9.46 mmol) of poly(VBTMA-Cl) aqueous solution (poly(VBTMA-Cl)/LiTFSI, 1/9 mol/mol). The reaction was carried out at room temperature for 48 h followed by washing with DI water for 72 h. The anion exchanged polymer, poly(VBTMA-TFSI), was filtered and dried under vacuum in an oven at room temperature for 24 h. The efficacy of anion exchange from Cl$^-$ to TFSI$^-$ was confirmed by EA and determined to be ~100% efficient. Yield: 3.1950 g (7.00 mmol) of solid polymer (74.0%). ^{1}H NMR (500 MHz, DMSO-d$_6$, 23 ℃) δ (ppm): 7.53-5.94 (m, 4H, C$_6$H$_4$), 4.64-3.77 (m, 2H, C$_6$H$_4$-C*H*$_2$-N), 3.17-2.39 (s,

9H, N-(CH_3)$_3$), 1.85−0.72 (s, 3H, CH_2-CH, CH$_2$-CH) (NMR, Figure 2.1). EA calculated: C, 36.84; H, 3.97; N, 6.14; Cl, 0.00; S, 14.05; F, 24.97. Found: C, 36.97; H, 3.83; N, 6.06; Cl, 0.00; S, 14.02; F, 24.84.

2.2.9 Synthesis of Poly(VBBIm-TFSI)

The non-ionic polymer, PVBC, was used as a precursor for the synthesis of styrene backbone PILs. The general procedure included functionalization of PVBC to form an ionic homopolymer followed by an anion exchange metathesis. The synthesis procedure of poly(VBBIm-TFSI) [VBBIm= vinylbenzylbutylimidazolium] is shown in Scheme 2.2 (2b(D)). An example reaction: 3.0046 g (19.69 mmol) of PVBC was dissolved in 35 mL DMF in a 125 mL flask. 12.20 g (98.24 mol) of 1-butylimidazole (PVBC/1-butylimidazole, 1/5 mol/mol) was slowly added dropwise into the flask. The reaction was carried out at 80 °C for 48 h. The resulting polymer was precipitated in hexane and subsequently washed in hexane multiple times. The solid polymer was dried under vacuum in an oven at room temperature for 24 h yielding 6.2785 g (22.68 mmol) light yellow solid particles (115.2%). Subsequently, anion exchange metathesis was performed on the dried polymer, poly(VBBIm-Cl), to exchange from Cl⁻ to TFSI⁻ form. 18.6270 g (64.9 mmol) of LiTFSI was stirred in 100 mL of DI water and added dropwise into 1.9999 g (7.22 mmol) of poly(VBBIm-Cl) aqueous solution (poly(VBBIm-Cl)/LiTFSI, 1/9 mol/mol). The reaction was carried out at room temperature for 48 h followed by washing with DI water for 72 h. The anion exchanged polymer, poly(VBBIm-TFSI), was filtered and dried under vacuum in an oven at room

temperature for 24 h. The efficacy of anion exchange from Cl⁻ to TFSI⁻ was confirmed

by EA and determined to be ~97% efficient. Yield: 3.2991g of solid polymer (87.6%).

^{1}H NMR (500 MHz, DMSO-d$_6$, 23 °C) δ (ppm): 9.39-9.09 (s,1H, N-C*H*=N), 7.88-7.59

(s, 2H, N-C*H*=C*H*-N), 7.57-6.01 (m, 4H, C$_6$*H*$_4$), 5.41-4.79 (m, 2H, C$_6$H$_4$-C*H*$_2$-N), 4.39-

3.86 (s, 2H, N-C*H*$_2$-CH$_2$-CH$_2$-CH$_3$), 1.83−1.56 (m, 3H, CH$_2$-C*H,* N-CH$_2$-C*H*$_2$-CH$_2$-CH$_3$),

1.56−0.93 (m, 4H, C*H*$_2$-CH, N-CH$_2$-CH$_2$-C*H*$_2$-CH$_3$), 0.93-0.58 (s, 3H, N-CH$_2$-CH$_2$-CH$_2$-

C*H*$_3$) (NMR, Figure 2.1). EA calculated: C, 41.46; H, 4.06; N, 8.06; Cl, 0.00; S, 12.30; F,

21.86. Found: C, 41.47; H, 4.03; N, 7.94; Cl, 0.00; S, 12.41; F, 21.68.

2.2.10 Synthesis of Poly(VBMP-TFSI)

The non-ionic polymer, PVBC, was used as a precursor for the synthesis of styrene

backbone PILs. The general procedure included functionalization of PVBC to form an

ionic homopolymer followed by an anion exchange metathesis. The synthesis procedure

of poly(VBMP-TFSI) [VBMP= vinylbenzylmethylpyrrolidinium] is shown in Scheme

2.2 (2b(E)). An example reaction: 0.9966 g (6.53 mmol) of PVBC was dissolved in 13

mL DMF in a 125 mL flask. 2.85 g (33.47 mol) of (PVBC/methylpyrrolidinium, 1/5

mol/mol) was slowly added dropwise into the flask. The reaction was carried out at room

temperature for 48 h. The resulting polymer was precipitated in hexane and subsequently

washed in hexane multiple times. The solid polymer was dried under vacuum in an oven

at room temperature for 24 h yielding 1.6478 g (6.93 mmol) yellow solid particles

(106.0%). Subsequently, anion exchange metathesis was performed on the dried polymer,

poly(VBMP-Cl), to exchange from Cl⁻ to TFSI⁻ form. 16.2930 g (56.75 mmol) of

28

LiTFSI was stirred in 100 mL of DI water and added dropwise into 1.5011 g (6.31 mmol) of poly(VBMP-Cl) aqueous solution (poly(VBMP-Cl)/LiTFSI, 1/9 mol/mol). The reaction was carried out at room temperature for 48 h followed by washing with DI water for 72 h. The anion exchanged polymer, poly(VBMP-TFSI), was filtered and dried under vacuum in an oven at room temperature for 24 h. The efficacy of anion exchange from Cl$^-$ to TFSI$^-$ was confirmed by EA and determined to be 98% efficient. Yield: 2.4402 g (5.06 mmol) of solid polymer (80.2%). ^{1}H NMR (500 MHz, acetonitrile-d$_3$, 23 °C) δ (ppm): 7.27-6.04 (m, 4H, C$_6$H$_4$), 4.48-3.83 (m, 2H, C$_6$H$_4$-CH$_2$-N), 3.58-2.92 (m, 4H, N-CH$_2$-CH$_2$-CH$_2$-CH$_2$-N), 2.87-2.35 (s, 4H, N-CH$_2$-CH$_2$-CH$_2$-CH$_2$-N), 2.32-1.82 (m, 4H, CH$_2$-CH, N-CH$_3$), 1.76-1.04 (m, 2H, CH$_2$-CH) (NMR, Figure 2.1). EA calculated: C, 39.83; H, 4.18; N, 5.81; Cl, 0.00; S, 13.29; F, 23.63. Found: C, 40.09; H, 4.14; N, 5.76; Cl, 0.00; S, 13.05; F, 23.37.

2.2.11 Characterization

The molecular weight and molecular weight distribution of poly(BrEMA) was performed with gel permeation chromatography (GPC) using a Waters GPC system (breeze 2) equipped with a THF Styragel column (Styragel@HR 5E, effective separation of molecular weight range: 2 to 4000 kg mol^{-1}) and a 2414 reflective index (RI) detector. GPC was calibrated with polystyrene standards (M$_w$: 2.97 to 983 kg mol^{-1}) and measured at 40 ℃ under a flow rate of 1.0 mL/min for the mobile phase (THF). Poly(BrEMA) was dissolved in THF to make 5 mg/mL solution.

Chemical analysis was performed with ^{1}H NMR spectroscopy (Varian Inova 500 MHz spectrometer) at room temperature with various NMR solvents. ^{1}H NMR spectra of BrEMA and poly(BrEMA) were collected referencing to CDCl$_3$ solvent at 7.27 ppm. Chemical shifts of poly(MEPip-TFSI), poly(MEBP-TFSI), poly(VBBP-TFSI) and poly(VBMP-TFSI) were collected referencing to acetonitrile-d$_3$ at 1.94 ppm. The measurements for the remaining PILs were performed using DMSO-d$_6$ as the NMR solvent and their chemical shifts were corrected referencing to 2.50 ppm.

Infrared spectroscopy was performed to determine the chemistries of all PILs. Experiments were performed at room temperature by a Fourier transform infrared (FTIR) spectrometer (Nicolet 6700 Series; Thermo Electron Corporation) using a single reflection diamond ATR accessory (Specac; Quest). All infrared spectra were collected using a liquid nitrogen-cooled mercury-cadmium-telluride (MCT) detector at 32 scans per spectrum and a resolution of 4 cm^{-1}. The collected spectra were corrected with a background subtraction of the spectrum of the bare ATR crystal.

Elemental analysis was performed by Atlantic Microlab, Inc. in Norcross, GA. Differential scanning calorimetry (DSC, TA Instruments, Q2000) was performed to determine glass transition temperatures (T$_g$s). The measurements were taken under nitrogen environment (50 mL/min) using a method of heat/cool/heat at a heating/ cooling rate of 10 °C /min over a temperature range of -140 to 180 °C. The T$_g$ was determined using the mid-point method on the second heating cycle thermogram. Thermal gravimetric analysis (TGA; TA Instruments, Q50) was performed on PILs to determine thermal degradation temperatures (T$_d$s). The measurements were taken under

nitrogen environment (60 mL/min) at a heating rate of 10 ℃/min over the temperature range of 25 to 900 ℃. The degradation temperature was determined at 5% weight loss.

2.3 Results and Discussion

2.3.1 Synthesis and Chemical Characterization of PILs

The non-ionic PIL precursor, poly(BrEMA), was synthesized *via* RAFT polymerization (shown in Scheme 2.2) and the ^{1}H NMR spectra is shown in Figure 2.1. Post-functionalization reactions with various cations were performed on poly(BrEMA) and poly(vinylbenzyl chloride) to achieve PILs (shown in Scheme 2.2). The resulting functionalized polymers, poly(MEBP-Br), poly(VBBIm-Cl), poly(VBTMA-Cl), poly(VBBP-Cl) and poly(VBMP-Cl) were found to be soluble in water. Therefore, water was chosen as solvent for anion exchange metathesis. The anion exchange reactions of poly(MEPip-Br) and poly(VBPip-Cl), which were insoluble in water, were also performed in water as solid-state anion exchange reactions. A typical procedure is also shown in Scheme 2.2. Chemical structures and purity of the TFSI-form of the PILs were confirmed with ^{1}H NMR spectroscopy and EA. ^{1}H NMR spectra of PILs are shown in Figure 2.1, which indicates that the PILs were almost fully functionalized and anion exchange metatheses were successful and highly efficient. Also, EA results further confirmed these results, where the compositions of the anion exchanged PILs are in close agreement with theory calculation, *i.e.*, bromide/chloride residues were negligibly small for methacrylate and styrene based PILs, respectively. This data provides evidence
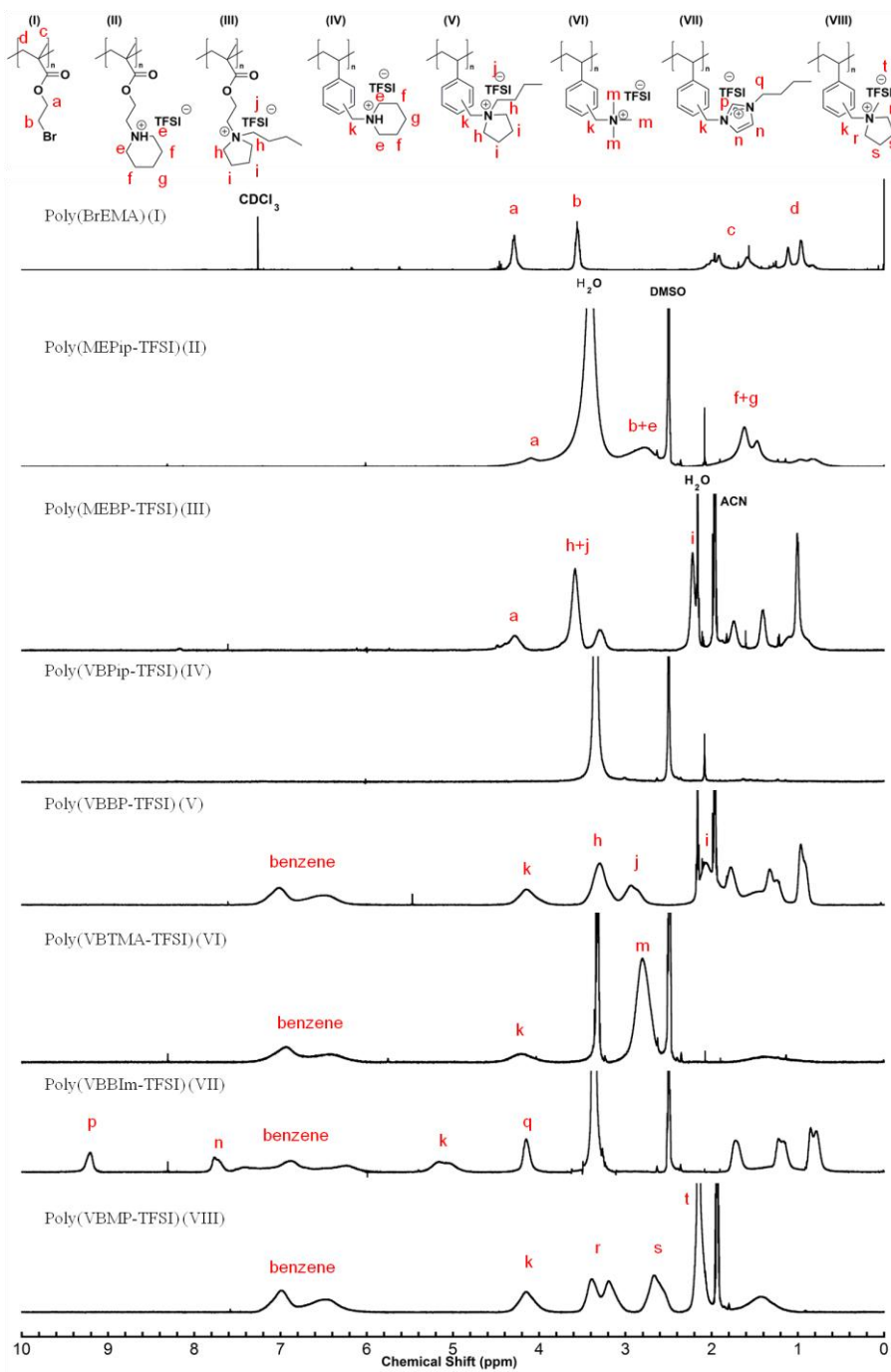
31

Figure 2.1 ^{1}H NMR spectra for (I) poly(BrEMA), (II) poly(MEPip-TFSI), (III) poly(MEBP-TFSI), (IV) poly(VBPip-TFSI), (V) poly(VBBP-TFSI), (VI) poly(VBTMA-TFSI), (VII) poly(VBBIm-TFSI), (VIII) poly(VBMP-TFSI).

that both liquid-state and solid-state anion exchange reactions achieved approximately fully exchanged PILs.

Infrared ATR spectra of all the PILs are showed in Figure 2.2. The characteristic infrared bands for TFSI$^-$ found in all PILs with TFSI anions: SO_2 stretching band (1346 cm^{-1},1053 cm^{-1}), CF_3 stretching band (1177, 1131 cm^{-1}), S-N-S stretching band (789 cm^{-1} and 741 cm^{-1}), antisymmetric CF_3 bending band (762 cm^{-1}). These bands are all consistent with TFSI anion assignments found in literature.[70] C-H stretching bands (3125, 2940, 2858 cm^{-1}) were found for piperidinium cation in the infrared spectra of poly(MEPip-TFSI) and poly(VBPip-TFSI), which are in close agreement with literature observations.[71] C-H stretching bands (3239, 2971, 2882 cm^{-1}) were found for butylpyrrolidinium cation in the infrared spectra of poly(MEBP-TFSI) and poly(VBBP-TFSI). C-H stretching bands (3148, 3112) and alkyl C-H stretching bands (2965, 2919, 2878, 2850 cm^{-1}) were found for the butylimidazolium cation in the infrared spectra of poly(VBBIm-TFSI), which are in close agreement with literature values.[72] C-H stretching bands (3254, 3047, 2928, 2857 cm^{-1}) were found for the trimethylammoniumcation in the infrared spectra of poly(VBTMA-TFSI). C-H stretching bands (3318, 2927 cm^{-1}) were found for the methylpyrrolidium cation in infrared spectra of poly(VBMP-TFSI).

Figure 2.2 Infrared spectra of PILs: poly(MEPip-TFSI) (black), poly(MEBP-TFSI) (blue), poly(VBPip-TFSI) (green), poly(VBBP-TFSI) (purple), poly(VBTMA-TFSI) (orange), poly(VBBIm-TFSI) (red) and poly(VBMP-TFSI) (Pink).

2.3.2 Thermal Properties of PILs

According to literature, the TFSI anion has a great influence on T_g depression after ion exchange from smaller halide anions, which can be resulted from the difference in size, lower symmetry, extensive charge delocalization,[73] and the flexibility of the TFSI anion.[74] DSC thermograms of all the polymers with TFSI as counterion are shown in Figure 2.3 and the glass transition temperatures (T_gs) are listed in Table 2.1. Among all the polymers, poly(VBBIm-TFSI) has the lowest T_g of 281 K, whereas poly(MEPip-TFSI) has the highest T_g of 375 K. T_gs in Table 2.1 suggest that the T_g is more strongly influenced by cation type than polymer backbone type, where the sequence of T_g values from low to high with different cation type as follows: butylimidazolium < butylpyrrolidium < methylpyrrolidinium < trimethylammonium < piperidium.
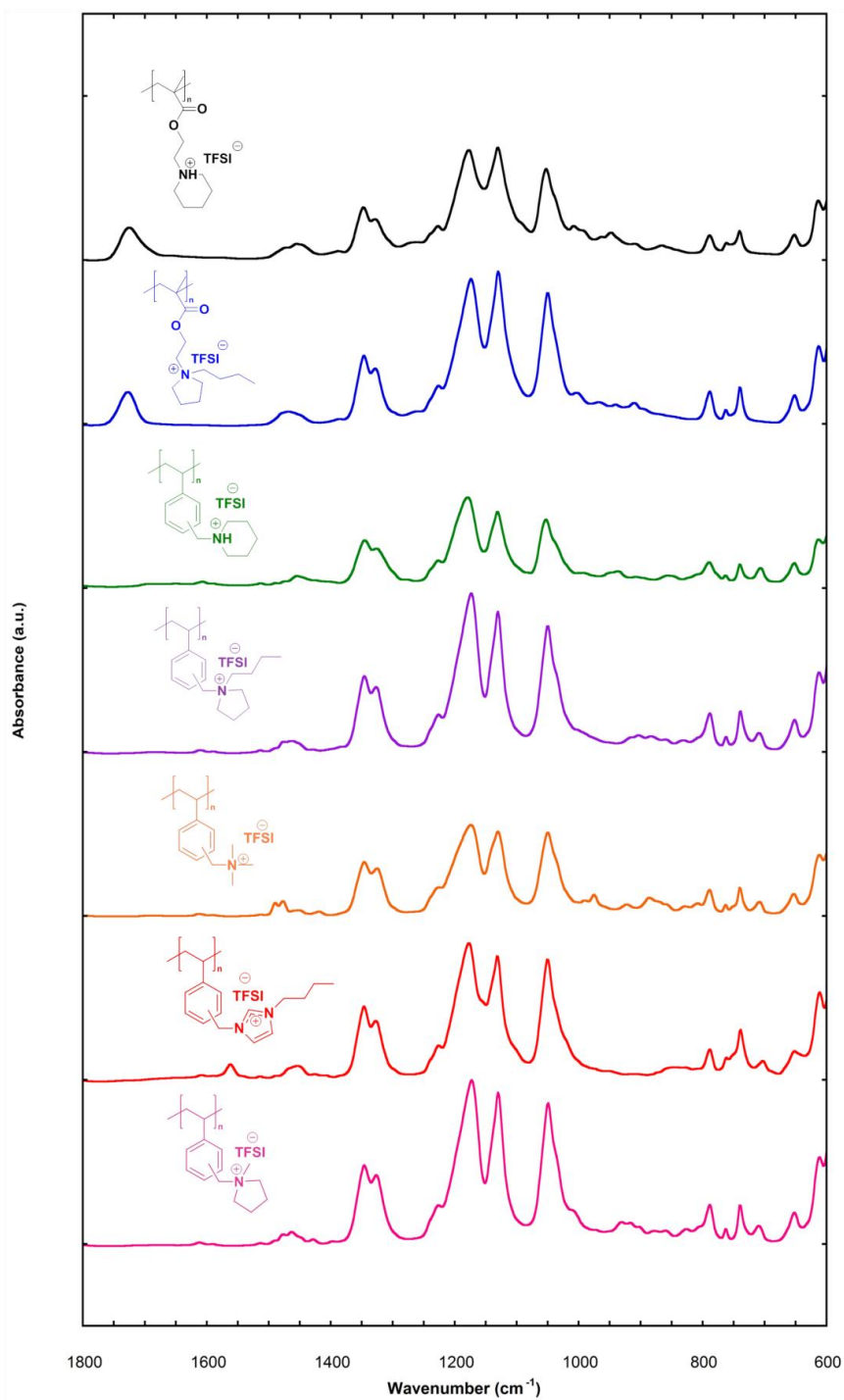
Figure 2.3 DSC thermograms of PILs: poly(MEPip-TFSI) (black), poly(MEBP-TFSI) (blue), poly(VBPip-TFSI) (green), poly(VBBP-TFSI) (purple), poly(VBTMA-TFSI) (orange), poly(VBBIm-TFSI) (red) and poly(VBMP-TFSI) (Pink). Arrows indicate mid-point location of thermal transition.

Figure 2.4 shows the thermal stability of PILs characterized by TGA under nitrogen environment. The thermal decomposition temperatures (T_ds) are listed in Table 2.1. Previous studies indicate that TFSI-exchanged PILs are found to undergo a one-step decomposition and show a higher decomposition temperature compared to other anions.[42] The TFSI anion is a weak, non-nucleophilic anion and one possible pathway for the decomposition of the TFSI anion is that it undergoes degradation *via* sulfur

36

dioxide release instead of dealkylation or proton transfer,[75] which makes it more difficult to thermally decompose. Data from Table 2.1 further confirmed the fact that PILs with TFSI anions are highly thermally stable, where TFSI-exchanged PILs have an average T_d of 585 K. T_ds in Table 2.1 suggest that thermal stability are more strongly correlated with differences in cations than polymer backbone, where the sequence of T_g values from low to high vary with cation type as follows: piperidium < butylpyrrolidium < trimethylammonium < metylpyrrolidium < butylimidazolium.
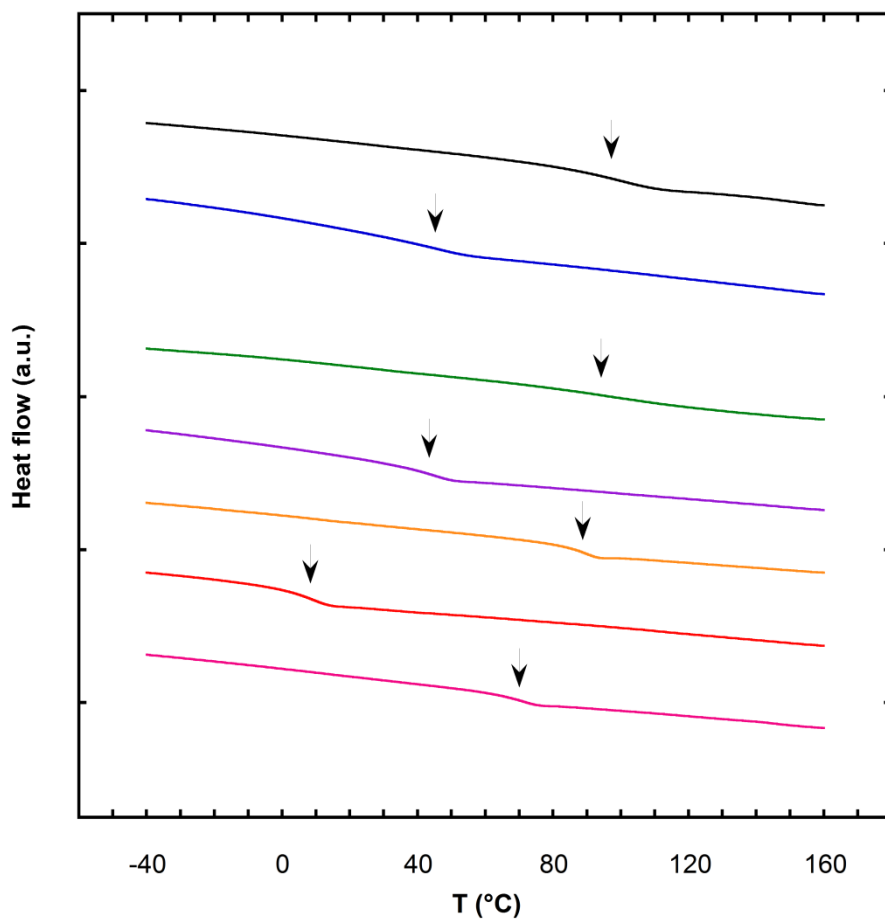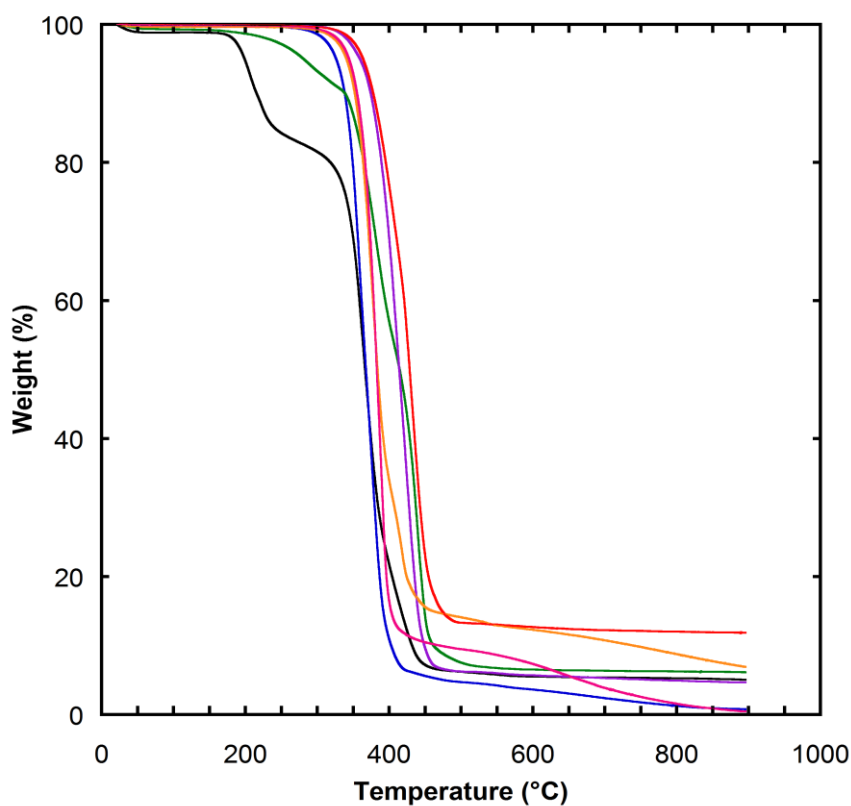

Figure 2.4 Thermal stability of PILs: poly(MEPip-TFSI) (black), poly(MEBP-TFSI) (blue), poly(VBPip-TFSI) (green), poly(VBBP-TFSI) (purple), poly(VBTMA-TFSI) (orange), poly(VBBIm-TFSI) (red) and poly(VBMP-TFSI) (pink).

Table 2.1 Thermal decomposition temperatures (T_ds) and glass transition temperatures (T_gs) of PILs.

PIL	T_d (K)	T_g (K)
poly(MEPip-TFSI)	473	375
poly(MEBP-TFSI)	599	322
poly(VBPip-TFSI)	554	368
poly(VBBP-TFSI)	603	317
poly(VBTMA-TFSI)	614	363
poly(VBBIm-TFSI)	637	282
Poly(VBMP-TFSI)	617	344

2.4 Conclusion

In this section, PILs with various backbone/cation pairings (backbones: ethyl methacrylate, styrene; covalently attached cations: butylimidazolium, trimethylammonium, piperidinium, butylpyrrolidinium, methylpyrrolidinium) were synthesized and characterized to investigate the influence of backbone and cation type on the chemistry and thermal properties. ^{1}H NMR and EA results confirm that functionalization and the anion exchange metathesis were successful and highly efficient. Chemical structures of all PILs were further investigated and confirmed with Fourier transform infrared spectroscopy. Glass transition temperatures of PILs differ with cation type significantly, where the sequence of T_g values vary from low to high with different cation type as: butylimidazolium < butylpyrrolidium < methylpyrrolidinium < trimethylammonium < piperidinium. Degradation temperatures differ with cation type significantly as well, where the sequence of T_d values vary from low to high with different cation type as: piperidinium < butylpyrrolidium < trimethylammonium <

methylpyrrolidium < butylimidazolium. Among all PILs, poly(VBBIm-TFSI) possesses

the lowest glass transition temperature (282 K) and highest degradation temperature (637

K). The carbonization of PILs will be described in Section 3.

3. POLYMERIZED IONIC LIQUID CARBONIZATION AND

CHARACTERIZATION

3.1 Introduction

Nitrogen-doped carbon have attracted investigations for several applications due to its outstanding properties, including high conductivity,[6,10] catalytic activity[11,12], *etc*. ILs possess outstanding physiochemical properties, such as negligible volatility, high ionic conductivity, and great chemical and thermal stability. By taking benefits from both the macromolecular structure and outstanding physiochemical properties of ILs, PILs are a promising candidate for nitrogen-doped carbon precursors. The resulting carbon material with high conductivity and high surface area are promising for numerous applications. Recently, several research groups have reported the ability to produce nitrogen-rich carbons from PILs.[37,57,67-69] However, few studies have explored the relationship between the possible diverse PIL chemistries and the resulting PIL-derived carbon properties. To achieve a more efficient PIL precursor synthesis for future applications, it is necessary to explore the influence of backbone and cation type and determine the promising chemistry for PIL-derived carbons as potential materials for future applications.

Previous work in Section 2 has shown the synthesis and characterizations of PILs as carbon precursors. In this section, poly(acrylonitrile) (PAN) was also synthesized as carbon precursor *via* RAFT (see Scheme 3.1) for a comparison (*i.e.*, control) . The chemistry and molecular weight of the PAN were characterized *via* ^{1}H NMR

spectroscopy. The thermal decomposition process of PAN was characterized by thermal gravimetric analysis (TGA). The carbonization of previous synthesized PILs and PAN were performed using TGA. Optical microscopy, scanning electron microscopy (SEM), transmission electron microscopy (TEM), X-ray diffraction (XRD) and X-ray photoelectron spectroscopy (XPS) were employed to investigate the properties of the resulting carbons. The results obtain a further understanding on the relationship between various chemistries of carbon precursors and the properties of resulting carbon.

3.2 Experimental Method

3.2.1 Materials

2-Cyano-2-propyl benzodithioate (CTA, >97%, HPLC), N, N-dimethylformamide (DMF, ACS Reagent, ≥99.8%), methanol (≥99.9%, HPLC), acetone (ACS reagent, ≥99.5%) was purchased from Sigma-Aldrich and used as received without further purification. Acrylonitrile (≥99%, contains 35-45 ppm monomethyl ether hydroquinone as inhibitor) was purified using a inhibitor removal column purchased from Sigma-Aldrich, azobis(isobutyronitrile) (AIBN, 98%, Sigma-Aldrich) was purified by recrystallization twice from methanol.

3.2.2 Synthesis of Poly(acrylonitrile)

RAFT polymerization was utilized to synthesize poly(acrylonitrile) (PAN) as a carbon precursor. The procedure is shown in Scheme 3.1. An example reaction: 25.08 g of

acrylonitrile (0.473 mol), 131.6 mg of CTA (0.595 mmol), 31.5 mg of AIBN (0.192 mmol) (acrylonitrile/CTA/AIBN, 800/1/0.1 mol/mol/mol), and 49.05 g N, N-dimethylformamide (DMF) were combined in a 250 mL single-neck Schlenk flask under continuous mixing. The reactor neck was well-sealed with septum and subjected to three freeze-pump-thaw degassing cycles. Followed by sealing the reactor arm and thawing in water bath, the reaction was carried out under N_2 at 75 ℃ for 20 h. The resulting polymer was precipitated in methanol, filtered and then dried under vacuum in an oven at room temperature for 24 h. Yield: 3.18 g of light yellow solid particles (12.67%). ^{1}H NMR (Mercury 300 MHz, DMSO-d$_6$, 23 °C) δ (ppm): 3.26-3.01 (s, 1H, CH_2-C*H*-C), 2.26-1.85 (m, 2H, C*H$_2$*-CH-CN) (NMR, Figure 3.1). M_n (NMR) = 23.83 kg mol^{-1}.

Scheme 3.1 Synthesis of PAN. (1) CTA, AIBN, 75 ℃, 20 h.
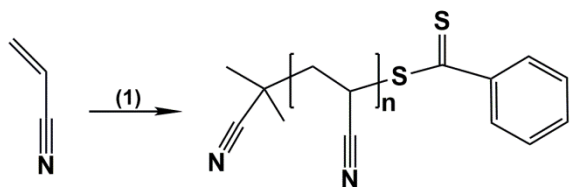
3.2.3 Carbonization of PAN

PAN was carbonized using thermal gravimetric analysis (TGA, TA Instruments, Q50). An example included placing 30 mg of PAN into a platinum pan and heating in the TGA up to 900 ℃ at a heating rate of 10 ℃/min under nitrogen environment (60 mL/min).

3.2.4 Carbonization of PILs

PILs were carbonized using thermal gravimetric analysis (TGA, TA Instruments, Q50). An example reaction of poly(MEPip-TFSI) carbonization included placing 60 mg of poly(MEPip-TFSI) into a platinum pan and heating in the TGA up to 900 ℃ at a heating rate of 10 ℃/min under nitrogen environment. The carbonizations of poly(VBPip-TFSI), poly(VBBP-TFSI), poly(VBTMA-TFSI), poly(VBBIm-TFSI) follow the same procedure as poly(MEPip-TFSI). The carbonization of poly(MEBP-TFSI) differed slightly from this procedure, where 60 mg of poly(MEBP-TFSI) were heated in the TGA up to 500 ℃ at a heating rate of 10 ℃/min under nitrogen environment.

3.2.5 Characterization

Carbon yield (%) was obtained using thermal gravimetric analysis (TGA; TA Instruments, Q50) on PAN and PILs. The measurements were taken under nitrogen environment (60 mL/min) at a heating rate of 10 ℃ /min over the temperature range of 25 to 900 ℃. Optical images were taken using a Zeiss Axiophot optical microscope using a 5X aperture. The surface structures and morphologies of the PAN or PIL derived carbons were characterized by scanning electron microscopy (SEM, FEI Quanta 600 FE-SEM) and transmission electron microscopy (TEM, JEOL JEM-2010). FE-SEM images were taken at 20 kV. Samples were loaded on carbon coated stubs and coated by sputtering Pt-Pd alloy prior to obtaining images. TEM images were taken at an acceleration voltage of 200 kV with LaB_6 filament. Samples were prepared in ethanol with sonication for 10 mins (40% amplitude, QSONICA Q125 sonicator). X-ray

diffraction (XRD) patterns were recorded on a Bruker-AXS D8 Advanced Bragg-Brentano X-ray powder diffractometer using Cu-K$_\alpha$ radiation (λ = 0.154 nm). Compositions of carbon products were measured by X-ray photoelectron spectroscopy (XPS). The measurements were performed on an Omicron XPS/UPS system with Argus detector using Omicron's DAR 400 dual Mg X-ray source.

3.3 Results and Discussion

3.3.1 Synthesis and Characterization of PAN

PAN was synthesized *via* RAFT polymerization (shown in Scheme 3.1). Chemical structure of PAN was confirmed with ^{1}H NMR spectroscopy and FTIR spectroscopy. Experimental details for ^{1}H NMR spectroscopy and FTIR spectroscopy are described in Section 2. The ^{1}H NMR spectrum (shown in Figure 3.1) indicates that PAN was successfully synthesized and the molecular weight was calculated to be 23.19 kg mol^{-1} using the integration ratio of repeating units to RAFT CTA.
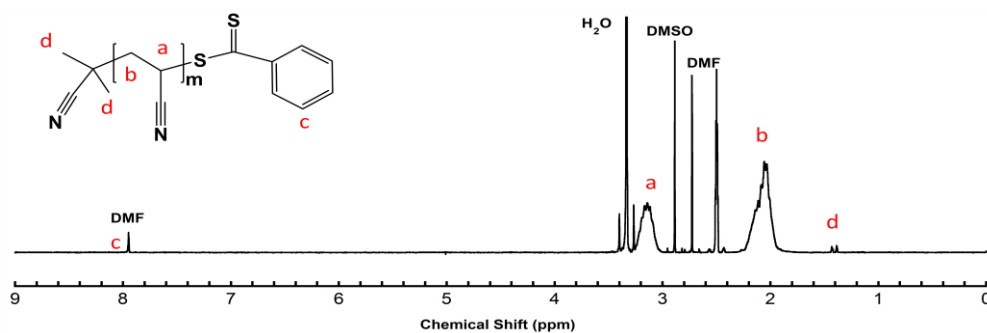

Figure 3.1 ^{1}H NMR (300 MHz) spectrum of PAN.

Infrared ATR spectrum of PAN is showed in Figure 3.2. The characteristic infrared bands for PAN found: $C \equiv N$ absorption bands: CN stretching band (2243 cm^{-1}), C-H stretching bands (2939 cm^{-1}, 2872 cm^{-1}), C-H bending bands (1454 cm^{-1}, 1358 cm^{-1}, 1248 cm^{-1}) were observed in the infrared spectra of PAN, which are in close agreement with literature.[76]
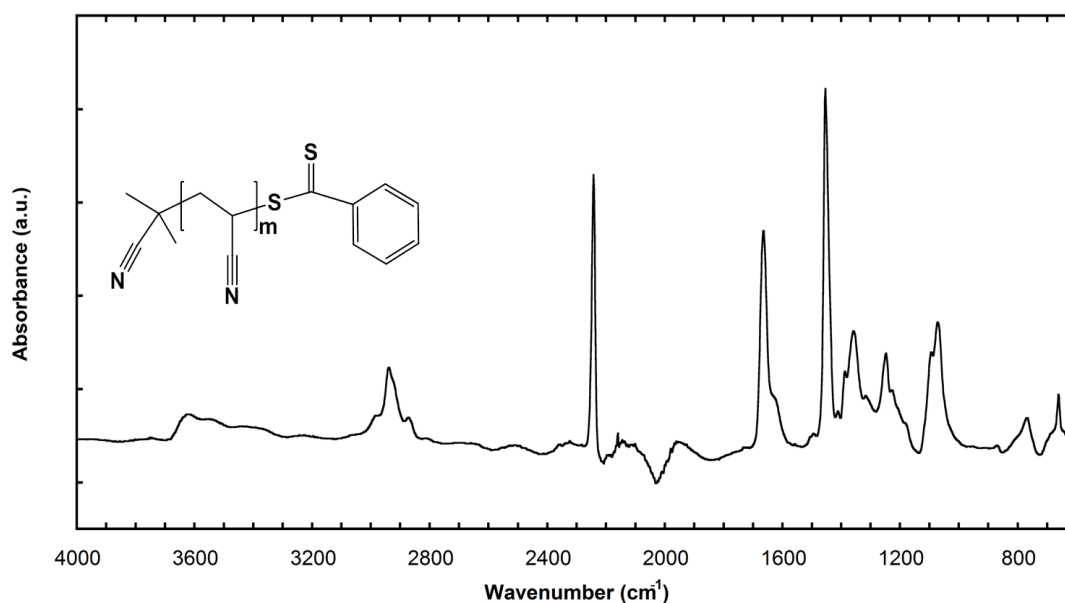
Figure 3.2 Infrared ATR spectrum of PAN at ambient conditions.

Figure 3.3 shows the thermal stability of PAN characterized by TGA under nitrogen environment. T_d of PAN at 5% weight loss is 270 ℃. Compared to the one-step decomposition of TFSI-exchanged PILs, the decomposition of PAN underwent a multi-step process. There were two main decomposition steps observed at 270 ℃ and 430 ℃, which agrees with the mechanisms described in literature.[77,78] Literature suggests the

45

degradation of PAN in the range of 270 to 400 ℃ produces HCN and water, while dehydrogenation occurs after 400 ℃.
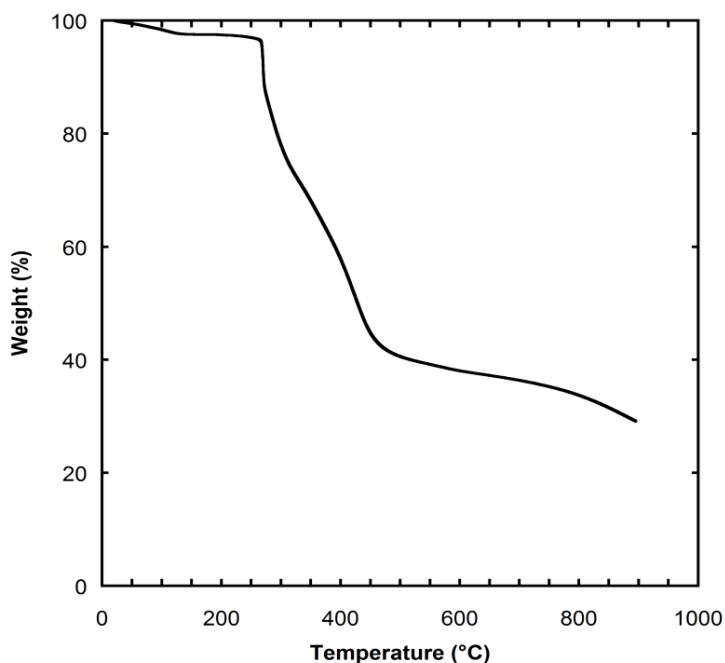
Figure 3.3 Thermal stability of PAN.

3.3.2 Carbon Yield

Carbon yield results were obtained from the TGA measurements performed on PAN and all PILs. The corresponding TGA curves for PILs and PAN are showed in Figure 2.4 and Figure 3.3, respectively. Table 3.1 lists the carbon yield from the pyrolysis at 900 ℃. PAN achieved the highest carbon yield (29.13%). For PILs, the carbon yield varied with backbone and cation type. For all styrene-based backbone PILs, the sequence of carbon yield values vary from low to high with different cation type as: methylpyrrolidium <

46

butylpyrrolidium < piperidium < trimethylammonium < butylimidazolium. When keeping the cation type the same, the styrene-based backbone provided a higher carbon yield compared to the methacrylate backbone. For poly(MEBP-TFSI), the carbon yield almost reached zero. As a result, the temperature for carbonization of poly(MEBP-TFSI) was changed to 500 ℃ to test the composition of carbon product.

Table 3.1 Carbon yield of PAN and PILs at 900 ℃.

Polymer	Residue (%)
PAN	29.13
poly(MEPip-TFSI)	5.04
poly(MEBP-TFSI)	0.183
poly(VBPip-TFSI)	6.12
poly(VBBP-TFSI)	4.90
poly(VBTMA-TFSI)	10.98
poly(VBBIm-TFSI)	11.84
poly(VBMP-TFSI)	0.441

3.3.3 Optical Microscopy

The optical images of the PAN derived carbon and PIL-derived carbons were taken by optical microscopy. Figure 3.4 shows the optical images of the carbon products derived from poly(MEBP-TFSI), poly(VBBP-TFSI), poly(VBTMA-TFSI), poly(VBBIm-TFSI) and PAN. The appearances of the resulting carbon materials were quite different. Carbonization of PAN contracted resulted in solid black powder; similar to what has

been observed in literature.[76] Carbonization of PILs resulted in something quite unexpected: carbon sheets. The resulting carbon materials possessed a metallic luster, suggesting a graphite structure may have been produced during pyrolysis. Slight appearance differences were also observed among different cation or backbone type.
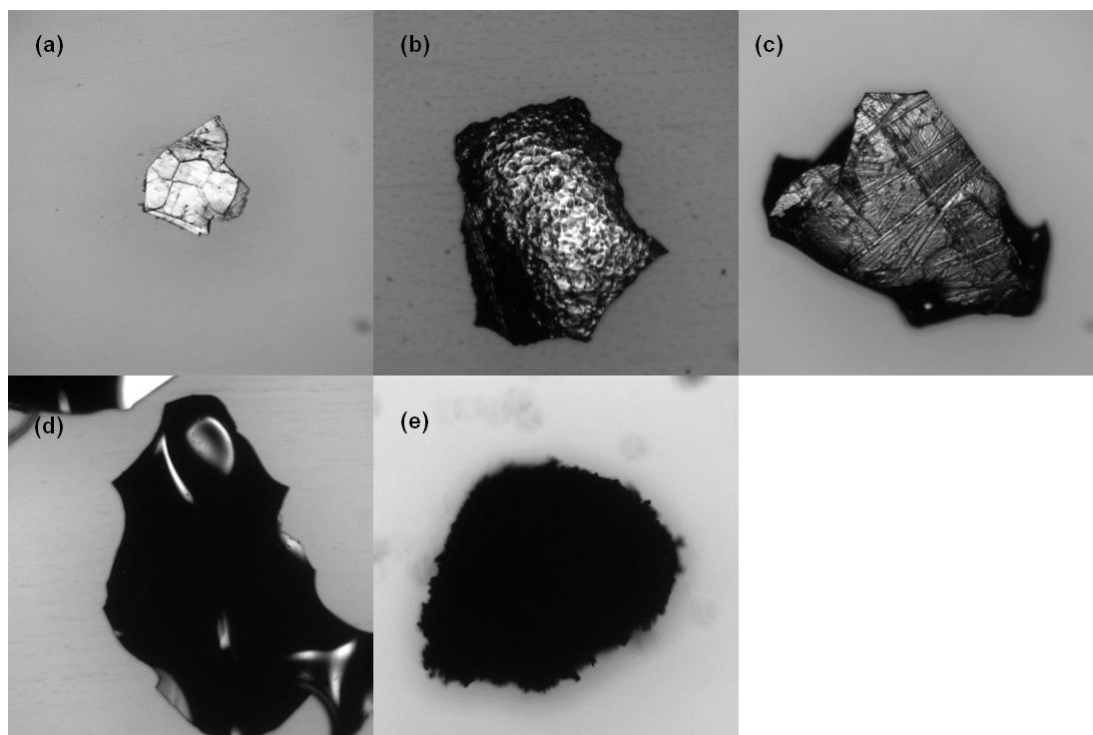

Figure 3.4 Optical images of the carbon material products derived from (a) poly(MEBP-TFSI) (b) poly(VBBP-TFSI) (c) poly(VBTMA-TFSI) (d) poly(VBBIm-TFSI) and (e) PAN.

3.3.4 Scanning Electron Microscopy (SEM)

The morphologies of the PAN-derived carbon and PIL-derived carbons were characterized by SEM. Figure 3.5 shows the SEM images of the carbon material products derived from poly(MEPip-TFSI), poly(MEBP-TFSI), poly(VBPip-TFSI), poly(VBBP-TFSI), poly(VBTMA-TFSI), poly(VBBIm-TFSI) and PAN. The SEM image of PAN-derived carbon (Figure 3.5 (g)) depicted a structure consisting of aggregation of particles, which suggests a broad particle size distribution. The structures changed significantly for PIL-derived carbons. Figure 3.5 (a) and Figure 3.5 (b) show the surface and edge structures of one piece of poly(MEPip-TFSI) and poly(MEBP-TFSI) derived carbon, respectively. The surfaces of both resulting carbons were smooth with some wavy patterns and the edge of poly(MEPip-TFSI) derived carbon showed porous structure inside the material. Figure 3.5 (c-f) showed that all styrene-based PILs derived carbons have smooth surfaces. However, the angle of the samples made it difficult to further focus the edges of pieces and determine the structure. Cross-section SEM may provide more information regarding the structure inside the carbon. However, it is difficult to take cross-section SEM images of the PIL-derived carbon due to their small brittle pieces. More attempts will be attempted in future investigations.
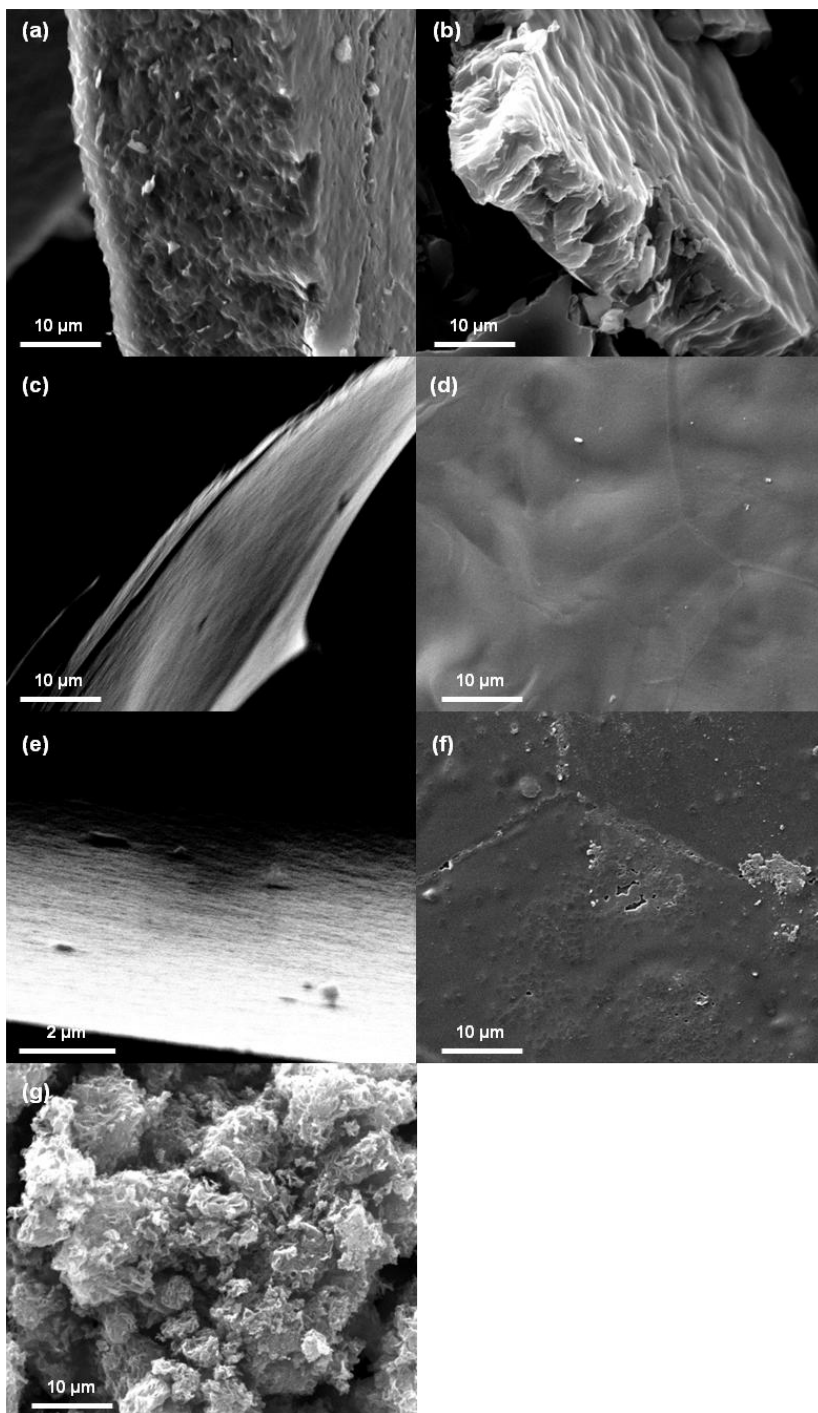
Figure 3.5 SEM images of the carbon material products derived from (a) poly(MEPip-TFSI) (b) poly(MEBP-TFSI) (c) poly(VBPip-TFSI) (d) poly(VBBP-TFSI) (e) poly(VBTMA-TFSI) (f) poly(VBBIm-TFSI) and (g) PAN.

3.3.5 Transmission Electron Microscopy (TEM)

The microstructure of the PAN-derived carbon and PIL-derived carbons were characterized by TEM. Figure 3.6 shows the TEM images of the carbon material products derived from poly(MEPip-TFSI), poly(MEBP-TFSI), poly(VBPip-TFSI), poly(VBBP-TFSI), poly(VBTMA-TFSI) and PAN. The carbonization for poly(MEBP-TFSI) was performed at 500 ℃, while the carbonization temperature for other polymers precursors was 900 ℃. In the sample preparation process, TFSI-formed PIL-derived carbons did not disperse well in solvents after sonication, while PAN-derived carbon dispersed well in ethanol within 2 min. This phenomenon was apparent in TEM images. Figure 3.6 (f) showed that the PAN-derived carbon possessed thin-layer morphology, while PIL-derived carbon was higher in density. Figure 3.6 (a) and Figure 3.6 (c) showed the morphologies difference between PILs with methacrylate-based backbone and styrene-based backbone, while having the same piperidinium cation. Comparable results were observed when comparing Figure 3.6 (b) and Figure 3.6 (d) for PILs with same butylpyrrolidinium cation. Carbon derived from methacrylate-based backbone PILs obtained smaller aggregation sizes, while the styrene-based backbone showed a compact multi-layer structure. The morphologies did not vary significantly when comparing styrene-based PILs with different cation type, which indicates that the cation type has a minor influence on the morphology.
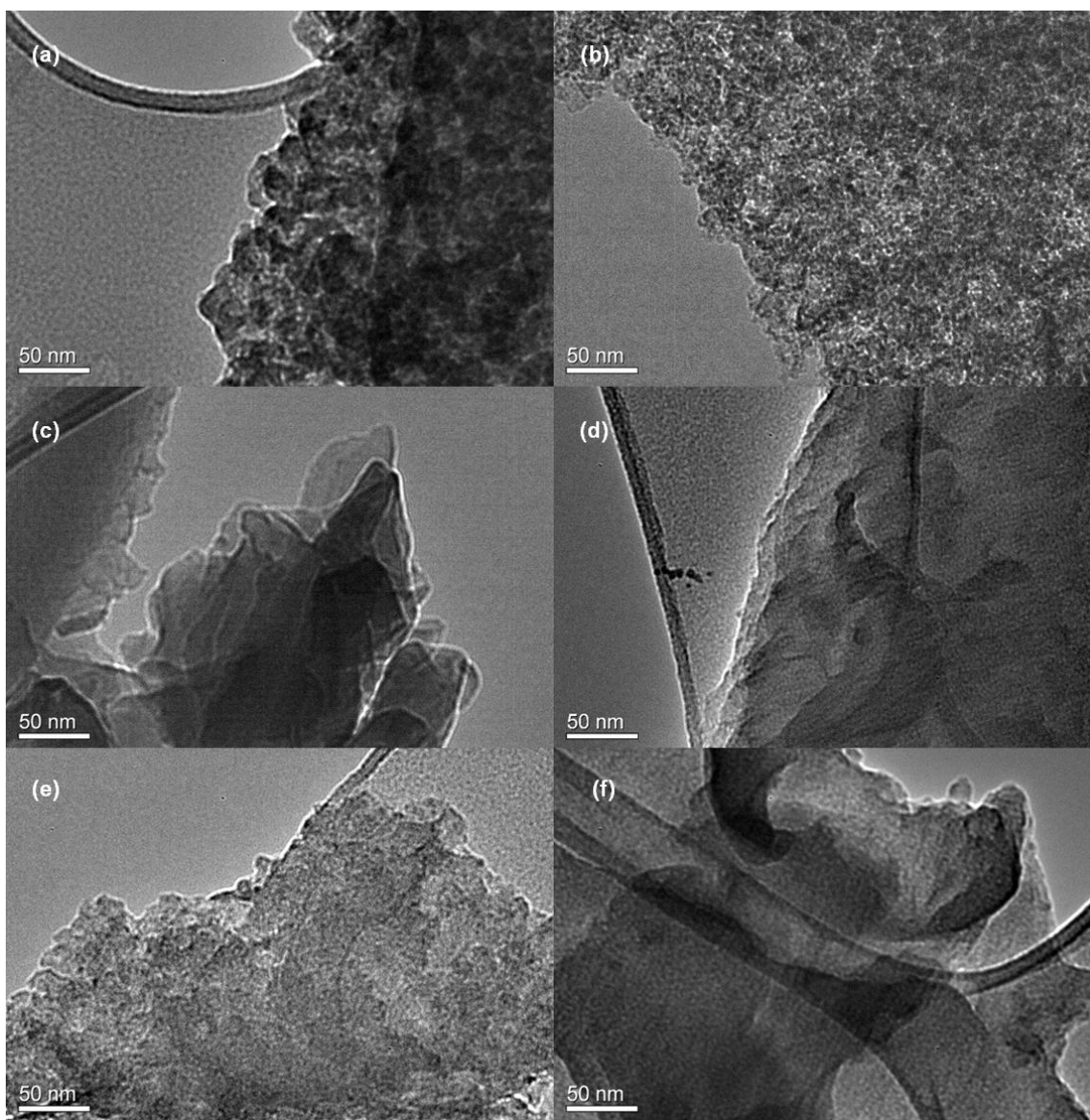
Figure 3.6 TEM images of the carbon material products derived from (a) poly(MEPip-TFSI) (b) poly(MEBP-TFSI) (c) poly(VBPip-TFSI) (d) poly(VBBP-TFSI) (e) poly(VBTMA-TFSI) and (f) PAN.

3.3.6 X-ray Diffraction (XRD)

XRD patterns show the phase and structure of PAN and PIL-derived carbons (Figure 3.7). Reflection bands at 26 ° and 44 ° were observed in the XRD patterns. All the peaks were broad with low intensity. Peaks at 26 ° ((002) plane reflection) and 44 ° ((100) plane reflection) are characteristic peaks of graphite structure and were observed in both PAN and PIL-derived carbons. The broad and noisy peaks indicated a less-ordered stacking of graphite layers due to the smaller graphitic regions and the local lattice distortion caused by nitrogen doping.[79] No obvious difference was observed between samples derived from different cation or backbone type.
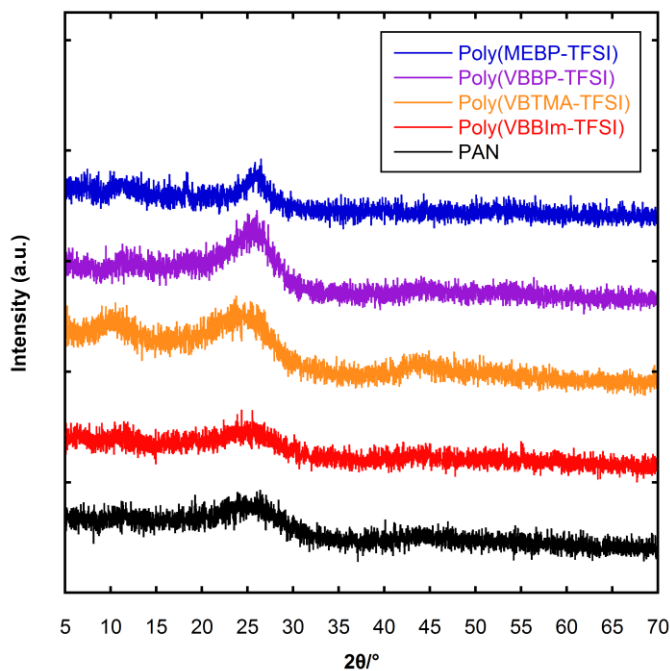

Figure 3.7 XRD patterns of the carbon material products derived from: poly(MEBP-TFSI) (blue), poly(VBBP-TFSI) (purple), poly(VBTMA-TFSI) (orange), poly(VBBIm-TFSI) (Red) and PAN (black).

3.3.7 X-ray Photoelectron Spectroscopy (XPS)

Table 3.2 showed the chemical composition of carbons derived from PAN and PILs. Poly(MEBP-TFSI) was prepared at 500 ℃ and the others were prepared at 900 ℃. From Figure 3.8, all the samples obtained peaks at 166, 285, 400 and 532 eV which were confirmed to be characteristic peaks for S 1s, C 1s, N 1s and O 1s spin orbits, respectively. The characteristic peak for F (689 eV) was found in most PIL-derived carbon samples. PAN-derived carbon possessed the highest nitrogen content of 6.97% with 26.42 wt% nitrogen content in the precursor. PIL-derived carbon possessed lower nitrogen contents of 1.44, 0.83, 1.06, 0.96 wt% for poly(MEBP-TFSI), poly(VBBP-TFSI), poly(VBTMA-TFSI), poly(VBBIm-TFSI) with precursor nitrogen contents of 5.04, 5.04, 6.06, 8.06 wt%, respectively. The low nitrogen contents are due to the low nitrogen content of precursor PILs. The percentage of retained nitrogen for poly(MEBP-TFSI), poly(VBBP-TFSI), poly(VBTMA-TFSI), poly(VBBIm-TFSI), and PAN are 28.57%, 16.47%, 17.49%, 11.91%, and 26.38%. Poly(MEBP-TFSI) possessed the highest nitrogen content among PIL-derived carbons. Also, when the carbonization temperature changed to 500 ℃, the sample obtained a high F content, which indicates that some of the degradation of the C-F bond may place after 500 ℃.

Table 3.2 XPS element composition of carbon derived from PAN and PILs.

	C (%)	O (%)	N (%)	S (%)	F (%)
Poly(MEBP-TFSI)	77.01	7.77	1.44	0.58	13.21

Table 3.2 Continued.

	C (%)	O (%)	N (%)	S (%)	F (%)
Poly(VBBP-TFSI)	90.58	6.78	0.83	1.50	0.31
Poly(VBTMA-TFSI)	89.87	7.93	1.06	1.01	0.14
Poly(VBBIm-TFSI)	85.33	12.26	0.96	1.46	0.00
PAN	86.36	5.99	6.97	0.68	0.00

Figure 3.8 shows the XPS spectra for PIL-drevided carbons. For poly(MEBP-TFSI), poly(VBBP-TFSI), poly(VBBIm-TFSI) derived carbons, the deconvolution of N 1s showed pyridinic N (398.7 eV) and pyrrolic N (400. 7 eV), which indicates that nitrogen atoms were structurally integrated into the carbon matrix of the resulting carbon materials and predominately in pyridinic and pyrrolic forms.[79,80] Graphitic N (402.1 eV) was also observed in poly(VBBIm-TFSI). In the spectra of poly(VBTMA-TFSI) derived carbon, N (401.2 eV) and a small amount of N (398.8 eV) was observed, indicating the structure of quaternary N and pyridinic N.[81] The data shows that the N component ratio varied with different cations on same styrene-based PIL precursors.
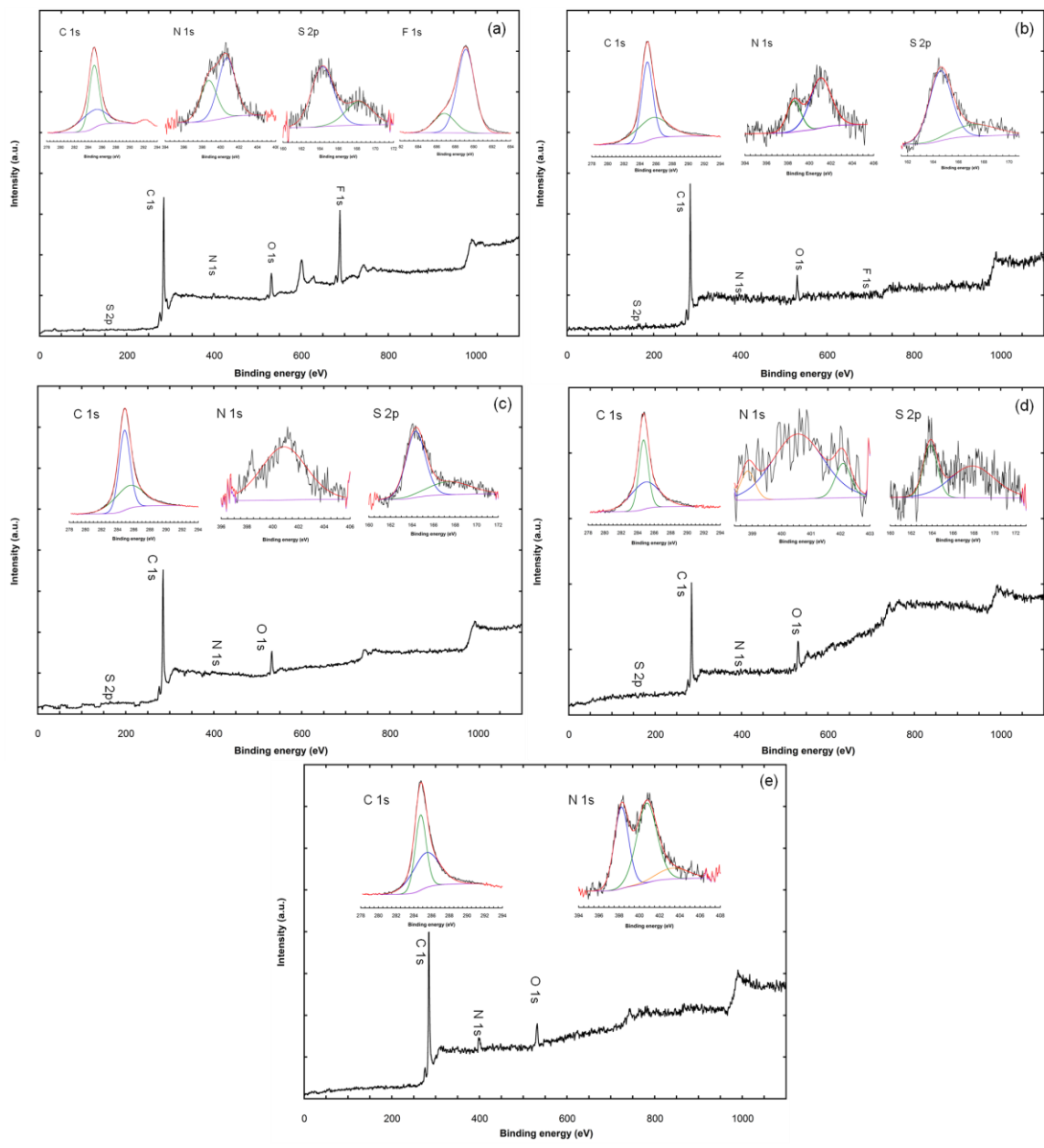
Figure 3.8 XPS spectra of the carbon material products derived from: (a) poly(MEBP-TFSI), (b) poly(VBBP-TFSI), (c) poly(VBTMA-TFSI), (d) poly(VBBIm-TFSI) and (e) PAN.

3.4 Conclusion

In this section, PILs with various backbone/cation pairings synthesized and characterized in Section 2 were carbonized to obtain nitrogen-doped carbon material. PAN was synthesized *via* RAFT polymerization as a comparison to PILs as nitrogen-doped carbon precursor. ^{1}H NMR confirmed that the synthesis was successful. Carbon yields were achieved from TGA, which suggests that cation type plays an important role in the resulting carbon yield. The sequence of carbon yield values vary from low to high with different cation type as: butylpyrrolidium < piperidinium < trimethylammonium < butylimidazolium. Also, styrene-based backbone provided a higher carbon yield compared to the methacrylate backbone.

The carbonization of previous synthesized PILs and PAN were successfully performed using TGA. Smooth surface were observed from the SEM images of all PIL-derived carbons. Wavy patterns and porous structure on the edges were observed from poly(MEPip-TFSI) derived carbon. TEM images showed that carbon derived from methacrylate-based backbone PILs obtained smaller aggregate sizes, while the styrene-based backbone showed a compact multi-layer structure. The morphologies did not vary significantly when comparing styrene-based PILs with different cation type, which indicates that the cation type has minor influence on the morphology.

XRD patterns showed two peaks at $26\,°$ and $44\,°$ indicative of a graphite structure obtained by all PAN and PILs derived carbons. XPS showed peaks of pyridinic N (398.7 eV) and pyrrolic N (400. 7 eV), which indicates that nitrogen atoms were structurally

integrated into the carbom matrix of the resulting carbon materials and predominately in pyridinic and pyrrolic forms.

4. CONCLUSION AND FUTURE OUTLOOK

4.1 Summary

This study demonstrates the synthesis and characterization of PILs as polymer precursors for nitrogen-doped carbon, a promising material for various applications, such as electrochemical devices and catalysts. The chemistries and thermal properties of PILs, as well as the morphologies and structures of the resulting carbons from pyrolysis were investigated. Further understanding has been achieved on the relationship between the chemistries of PILs and the properties of resulting carbons for more targeted future synthesis.

PILs with various backbone/cation pairings (backbones: ethyl methacrylate, styrene; covalently attached cations: butylimidazolium, trimethylammonium, piperidinium, butylpyrrolidinium, methylpyrrolidinium) were synthesized and characterized to investigate the influence of backbone and cation type on the chemistry and thermal properties. Thermal properties of PILs differ with cation type significantly, where the sequence of glass transition temperature values vary from low to high with different cation type as: butylimidazolium < butylpyrrolidium < methylpyrrolidinium < trimethylammonium < piperidium and the sequence of degradation temperature values vary from low to high with different cation type as: piperidium < butylpyrrolidium < trimethylammonium < butylimidazolium.

PAN was synthesized *via* RAFT polymerization as a comparison to PILs as nitrogen-doped carbon precursor. PILs and PAN were carbonized at 900 °C. Cation type plays an

important role in the resulting carbon yield, where the sequence of carbon yield values vary from low to high with different cation type as: butylpyrrolidium < piperidium < trimethylammonium < butylimidazolium. Also, styrene-based backbone provided a higher carbon yield compared to the methacrylate backbone.

The morphologies of resulting carbon materials depends more on backbone type than cation type. Small particle aggregation with porous structure was observed for methcrylate derived carbon, while a compact multi-layer structure with smooth surfaces were observed from styrene based carbons. Graphitic structure was observed by XRD patterns for all PAN and PIL-derived carbons. XPS showed peaks of pyridinic N (398.7 eV) and pyrrolic N (400. 7eV), which indicates that N atoms were structurally integrated into the carbom matrix of the resulting carbon materials and predominately in pyridinic and pyrrolic forms.

4.2 Future Outlook

Multiple possibilities and directions can be investigated in the future beyond the work showed in this thesis. In this study, we only focused on investigating the morphology of resulting carbon materials and its relationship with the chemistry of polymer precursor. More characterization is necessary to determine the composition, pore size, surface area, conductivity and electrochemical performance of the resulting carbons to obtain a better understanding on the influence of cation type and backbone type. To achieve this goal, first and foremost, it is of great importance to realize larger batch carbonization reactions. Currently the reactions were performed in TGA, where only a small amount of polymer

precursor can be used for carbonization. This resulted in the limit amount of obtained product from the carbonization and further constrained essential characterization data that could be obtained. Elemental analysis can be performed to determine the composition of resulting carbon material and the results can be compared to the XPS results. Nitrogen sorption measurements are necessary to investigate the specific surface area and the pore size distribution. Cross-section SEM, high resolution TEM and Raman spectroscopy will also be included in the future to further compare the morphology achieved by different cation type and backbone type.

Besides additional characterization methods, anion type can be another direction to explore in future studies. In this study, the influences of cation type and backbone type have been investigated. Anion type has been reported to play an important role in affecting the porosity of IL-derived carbons.[82] More anion types and their effect on porosity of PIL-derived carbon can be investigated to determine the best PIL chemistry for high surface carbon material.

In this study, nitrogen contents of PIL-derived carbon materials were not as high as the control PAN-derived carbon. This was a result of lower nitrogen contents in the PIL precursors. In order to achieve nitrogen-doped carbon with high nitrogen content, more nitrogen can be introduced into the backbone chemistry. PAN-b-X-b-PIL block polymers (where X is a degradable polymer) can also be considered as a promising carbon precursor to obtain nitrogen-doped carbon with the combination of high carbon yield, high nitrogen content, and a highly well-controlled nano-porous structure.

REFERENCES

(1)   Frackowiak, E.; Beguin, F. *Carbon* **2001**, *39*, 937.

(2)   Zhai, Y. P.; Dou, Y. Q.; Zhao, D. Y.; Fulvio, P. F.; Mayes, R. T.; Dai, S. *Adv. Mater.* **2011**, *23*, 4828.

(3)   Robertson, J. *Mater. Sci. Eng. R-Rep.* **2002**, *37*, 129.

(4)   Baughman, R. H.; Zakhidov, A. A.; de Heer, W. A. *Science* **2002**, *297*, 787.

(5)   Lozano-Castello, D.; Cazorla-Amoros, D.; Linares-Solano, A.; Shiraishi, S.; Kurihara, H.; Oya, A. *Carbon* **2003**, *41*, 1765.

(6)   Frackowiak, E. *Physical Chemistry Chemical Physics* **2007**, *9*, 1774.

(7)   Zhang, L. L.; Zhao, X. S. *Chem. Soc. Rev.* **2009**, *38*, 2520.

(8)   Simon, P.; Gogotsi, Y. *Nat Mater* **2008**, *7*, 845.

(9)   Pandolfo, A. G.; Hollenkamp, A. F. *Journal of Power Sources* **2006**, *157*, 11.

(10)   Seredych, M.; Hulicova-Jurcakova, D.; Lu, G. Q.; Bandosz, T. J. *Carbon* **2008**, *46*, 1475.

(11)   Yang, W.; Fellinger, T. P.; Antonietti, M. *J Am Chem Soc* **2011**, *133*, 206.

(12)   Elumeeva, K.; Fechler, N.; Fellinger, T. P.; Antonietti, M. *Mater. Horizons* **2014**, *1*, 588.

(13)   Wei, J.; Zhou, D. D.; Sun, Z. K.; Deng, Y. H.; Xia, Y. Y.; Zhao, D. Y. *Adv. Funct. Mater.* **2013**, *23*, 2322.

(14)   Hulicova-Jurcakova, D.; Seredych, M.; Lu, G. Q.; Bandosz, T. J. *Adv. Funct. Mater.* **2009**, *19*, 438.

(15)   Jeong, H. M.; Lee, J. W.; Shin, W. H.; Choi, Y. J.; Shin, H. J.; Kang, J. K.; Choi, J. W. *Nano Lett.* **2011**, *11*, 2472.

(16)   Ania, C. O.; Khomenko, V.; Raymundo-Pinero, E.; Parra, J. B.; Beguin, F. *Adv. Funct. Mater.* **2007**, *17*, 1828.

(17)   Hulicova-Jurcakova, D.; Kodama, M.; Shiraishi, S.; Hatori, H.; Zhu, Z. H.; Lu, G. Q. *Adv. Funct. Mater.* **2009**, *19*, 1800.

(18)   Li, Z.; Xu, Z. W.; Tan, X. H.; Wang, H. L.; Holt, C. M. B.; Stephenson, T.; Olsen, B. C.; Mitlin, D. *Energy Environ. Sci.* **2013**, *6*, 871.

(19)   Su, F.; Poh, C. K.; Chen, J. S.; Xu, G.; Wang, D.; Li, Q.; Lin, J.; Lou, X. W. *Energy Environ. Sci.* **2011**, *4*, 717.

(20)   Hulicova, D.; Yamashita, J.; Soneda, Y.; Hatori, H.; Kodama, M. *Chem Mater* **2005**, *17*, 1241.

(21)   Wen, Z.; Wang, X.; Mao, S.; Bo, Z.; Kim, H.; Cui, S.; Lu, G.; Feng, X.; Chen, J. *Adv. Mater.* **2012**, *24*, 5610.

(22)   Hassan, F. M.; Chabot, V.; Li, J.; Kim, B. K.; Ricardez-Sandoval, L.; Yu, A. *Journal of Materials Chemistry A* **2013**, *1*, 2904.

(23)   Kim, N. D.; Kim, W.; Joo, J. B.; Oh, S.; Kim, P.; Kim, Y.; Yi, J. *Journal of Power Sources* **2008**, *180*, 671.

(24)   Jurewicz, K.; Babel, K.; Ziolkowski, A.; Wachowska, H. *Electrochimica Acta* **2003**, *48*, 1491.

(25)   Sheng, Z.-H.; Shao, L.; Chen, J.-J.; Bao, W.-J.; Wang, F.-B.; Xia, X.-H. *ACS Nano* **2011**, *5*, 4350.

(26)   Lee, Y. H.; Lee, Y. F.; Chang, K. H.; Hu, C. C. *Electrochem. Commun.* **2011**, *13*, 50.

(27)   Wu, Y.; Fang, S.; Jiang, Y. *Journal of Power Sources* **1998**, *75*, 201.

(28)   Park, J.-H.; Ju, Y.-W.; Park, S.-H.; Jung, H.-R.; Yang, K.-S.; Lee, W.-J. *Journal of Applied Electrochemistry* **2009**, *39*, 1229.

(29)   Zhong, M.; Kim, E. K.; McGann, J. P.; Chun, S.-E.; Whitacre, J. F.; Jaroniec, M.; Matyjaszewski, K.; Kowalewski, T. *J Am Chem Soc* **2012**, *134*, 14846.

(30)   Walden, P. *Bulletin of the Russian Academy of Sciences* **1914**, 405.

(31)   Parvulescu, V. I.; Hardacre, C. *Chem. Rev.* **2007**, *107*, 2615.

(32)   Kubisa, P. *Prog. Polym. Sci.* **2004**, *29*, 3.

(33)   Wilkes, J. S.; Levisky, J. A.; Wilson, R. A.; Hussey, C. L. *Inorg. Chem.* **1982**, *21*, 1263.

(34)   Armand, M.; Endres, F.; MacFarlane, D. R.; Ohno, H.; Scrosati, B. *Nat. Mater.* **2009**, *8*, 621.

(35)   Liu, J. F.; Jonsson, J. A.; Jiang, G. B. *Trac-Trends Anal. Chem.* **2005**, *24*, 20.

(36)   Paraknowitsch, J. P.; Zhang, J.; Su, D. S.; Thomas, A.; Antonietti, M. *Adv. Mater.* **2010**, *22*, 87.

(37)   Yuan, J. Y.; Giordano, C.; Antonietti, M. *Chem Mater* **2010**, *22*, 5003.

(38)   Fellinger, T.-P.; Thomas, A.; Yuan, J.; Antonietti, M. *Advanced Materials* **2013**, *25*, 5838.

(39)   Fechler, N.; Fellinger, T. P.; Antonietti, M. *Chem Mater* **2012**, *24*, 713.

(40)   Ohno, H.; Ito, K. *Chem Lett* **1998**, 751.

(41)   Meek, K. M.; Elabd, Y. A. *Journal of Materials Chemistry A* **2015**, *3*, 24187.

(42)   Ye, Y.; Elabd, Y. A. *Polymer* **2011**, *52*, 1309.

(43)   Hirao, M.; Ito, K.; Ohno, H. *Electrochimica Acta* **2000**, *45*, 1291.

(44)   Shaplov, A. S.; Lozinskaya, E. I.; Ponkratov, D. O.; Malyshkina, I. A.; Vidal, F.; Aubert, P.-H.; Okatova, O. g. V.; Pavlov, G. M.; Komarova, L. I.; Wandrey, C.; Vygodskii, Y. S. *Electrochimica Acta* **2011**, *57*, 74.

(45)   Matsumoto, K.; Talukdar, B.; Endo, T. *Polymer Bulletin* **2011**, *66*, 199.

(46)   Cardiano, P.; Mineo, P. G.; Neri, F.; Lo Schiavo, S.; Piraino, P. *J Mater Chem* **2008**, *18*, 1253.

(47)   Zhang, Y. *Chemical Biology & Drug Design* **2009**, *74*, 282.

(48)   Tang, H. D.; Tang, J. B.; Ding, S. J.; Radosz, M.; Shen, Y. Q. *J Polym Sci Pol Chem* **2005**, *43*, 1432.

(49)   Ding, S. J.; Tang, H. D.; Radosz, M.; Shen, Y. Q. *J Polym Sci Pol Chem* **2004**, *42*, 5794.

(50)   He, H. K.; Luebke, D.; Nuwala, H.; Matyjaszewski, K. *Macromolecules* **2014**, *47*, 6601.

(51)   He, H. K.; Averick, S.; Roth, E.; Luebke, D.; Nulwala, H.; Matyjaszewski, K. *Polymer* **2014**, *55*, 3330.

(52)   He, X.; Yang, W.; Pei, X. *Macromolecules* **2008**, *41*, 4615.

(53)   He, H. K.; Zhong, M. J.; Luebke, D.; Nulwala, H.; Matyjaszewski, K. *J Polym Sci Pol Chem* **2014**, *52*, 2175.

(54)   Vijayakrishna, K.; Jewrajka, S. K.; Ruiz, A.; Marcilla, R.; Pomposo, J. A.; Mecerreyes, D.; Taton, D.; Gnanou, Y. *Macromolecules* **2008**, *41*, 6299.

(55)   Mori, H.; Yahagi, M.; Endo, T. *Macromolecules* **2009**, *42*, 8082.

(56)   Zhang, Q.; Zhu, S. P. *ACS Macro Lett.* **2015**, *4*, 755.

(57)   Yuan, J. Y.; Schlaad, H.; Giordano, C.; Antonietti, M. *Eur Polym J* **2011**, *47*, 772.

(58)   Meek, K. M.; Sharick, S.; Ye, Y. S.; Winey, K. I.; Elabd, Y. A. *Macromolecules* **2015**, *48*, 4850.

(59)   Nykaza, J. R.; Ye, Y. S.; Elabd, Y. A. *Abstr Pap Am Chem S* **2014**, *247*.

(60)   Karjalainen, E.; Chenna, N.; Laurinmaki, P.; Butcher, S. J.; Tenhu, H. *Polymer Chemistry* **2013**, *4*, 1014.

(61)   Sudre, G.; Inceoglu, S.; Cotanda, P.; Balsara, N. P. *Macromolecules* **2013**, *46*, 1519.

(62)   Long, S. J.; Wan, F.; Yang, W.; Guo, H.; He, X. Y.; Ren, J.; Gao, J. Z. *J Appl Polym Sci* **2013**, *128*, 2687.

(63)   Weber, R. L.; Ye, Y. S.; Schmitt, A. L.; Banik, S. M.; Elabd, Y. A.; Mahanthappa, M. K. *Macromolecules* **2011**, *44*, 5727.

(64)   Yang, Y. T.; Knauss, D. M. *Macromolecules* **2015**, *48*, 4471.

(65)   Yang, W.; He, X. J.; Gao, J. Z.; Guo, H.; He, X. Y.; Wan, F.; Zhao, X. L.; Yu, Y.; Pei, B. *Chin. Sci. Bull.* **2010**, *55*, 3562.

(66)   Szwarc, M. *Nature* **1956**, *178*, 1168.

(67)   Yuan, J.; Marquez, A. G.; Reinacher, J.; Giordano, C.; Janek, J.; Antonietti, M. *Polymer Chemistry* **2011**, *2*, 1654.

(68)   Kuzmicz, D.; Coupillaud, P.; Men, Y.; Vignolle, J.; Vendraminetto, G.; Ambrogi, M.; Taton, D.; Yuan, J. Y. *Polymer* **2014**, *55*, 3423.

(69)   Zhao, Q.; Fellinger, T. P.; Antonietti, M.; Yuan, J. Y. *Journal of Materials Chemistry A* **2013**, *1*, 5113.

(70)   Seki, T.; Grunwaldt, J.-D.; Baiker, A. *The Journal of Physical Chemistry B* **2009**, *113*, 114.

(71)   Shukla, M.; Saha, S. In *Ionic Liquids - New Aspects for the Future*; Kadokawa, J.-i., Ed.; InTech: Rijeka, Croatia, **2013**; Chapter 3.

(72)   Zheng, Y.-Z.; Wang, N.-N.; Luo, J.-J.; Zhou, Y.; Yu, Z.-W. *Physical Chemistry Chemical Physics* **2013**, *15*, 18055.

(73)   Benrabah, D.; Arnaud, R.; Sanchez, J. Y. *Electrochimica Acta* **1995**, *40*, 2437.

(74)   Arnaud, R.; Benrabah, D.; Sanchez, J. Y. *Journal of Physical Chemistry* **1996**, *100*, 10882.

(75)   Kroon, M. C.; Buijs, W.; Peters, C. J.; Witkamp, G. J. *Thermochim. Acta* **2007**, *465*, 40.

(76)   Korobeinyk, A. V.; Whitby, R. L. D.; Mikhalovsky, S. V. *Eur Polym J* **2012**, *48*, 97.

(77)   Xue, T. J.; McKinney, M. A.; Wilkie, C. A. *Polymer Degradation and Stability* **1997**, *58*, 193.

(78)   Grassie, N.; McGuchan, R. *Eur Polym J* **1970**, *6*, 1277.

(79)   Wang, L.; Gao, Z. Y.; Chang, J. L.; Liu, X.; Wu, D. P.; Xu, F.; Guo, Y. M.; Jiang, K. *ACS Applied Materials & Interfaces* **2015**, *7*, 20234.

(80)   Artyushkova, K.; Kiefer, B.; Halevi, B.; Knop-Gericke, A.; Schlogl, R.; Atanassov, P. *Chemical Communications* **2013**, *49*, 2539.

(81)   Chambrion, P.; Suzuki, T.; Zhang, Z.-G.; Kyotani, T.; Tomita, A. *Energy & Fuels* **1997**, *11*, 681.

(82)   Lee, J. S.; Wang, X. Q.; Luo, H. M.; Baker, G. A.; Dai, S. *J Am Chem Soc* **2009**, *131*, 4596.